Published in final edited form as:
J Photochem Photobiol B. 2010 January 21; 98(1): 77–94. doi:10.1016/j.jphotobiol.2009.11.007.

Preclinical Whole-body Fluorescence Imaging: Review of Instruments, Methods and Applications

Frederic Leblond[1,*,&], **Scott C. Davis**[1], **Pablo A. Valdés**[1], and **Brain W. Pogue**[1,2,&]
[1]Thayer School of Engineering, Dartmouth College, Hanover NH 03755, USA
[2]Department of Surgery, Dartmouth Medical School, Lebanon, NH 03756

Abstract

Fluorescence sampling of cellular function is widely used in all aspects of biology, allowing the visualization of cellular and sub-cellular biological processes with spatial resolutions in the range from nanometers up to centimeters. Imaging of fluorescence in vivo has become the most commonly used radiological tool in all pre-clinical work. In the last decade, full-body pre-clinical imaging systems have emerged with a wide range of utilities and niche application areas. The range of fluorescent probes that can be excited in the visible to near-infrared part of the electromagnetic spectrum continues to expand, with the most value for in vivo use being beyond the 630 nm wavelength, because the absorption of light sharply decreases. Whole-body in vivo fluorescence imaging has not yet reached a state of maturity that allows its routine use in the scope of large-scale pre-clinical studies. This is in part due to an incomplete understanding of what the actual fundamental capabilities and limitations of this imaging modality are. However, progress is continuously being made in research laboratories pushing the limits of the approach to consistently improve its performance in terms of spatial resolution, sensitivity and quantification. This paper reviews this imaging technology with a particular emphasis on its potential uses and limitations, the required instrumentation, and the possible imaging geometries and applications. A detailed account of the main commercially available systems is provided as well as some perspective relating to the future of the technology development. Although the vast majority of applications of in vivo small animal imaging are based on epi-illumination planar imaging, the future success of the method relies heavily on the design of novel imaging systems based on state-of-the-art optical technology used in conjunction with high spatial resolution structural modalities such as MRI, CT or ultra-sound.

Keywords

fluorescence; imaging; tomography; commercial; molecular; fluorophore; small animal; diagnostic

[*]**Correspondence to:** Thayer School of Engineering Dartmouth College Hanover NH 03755 USA Tel: (603) 646-2100 Fax: (603) 646-3856 frederic.leblond@dartmouth.edu.
[&]**Disclaimer:** Authors F. Leblond and B. W. Pogue have been consultants for ART Inc in the past, one of the suppliers of an imaging system reviewed in this paper.

1. Introduction

Many researchers in the biological sciences appreciate the extraordinary contrast and specificity provided by fluorescence microscopy. Extrapolating this imaging paradigm to whole-body animal imaging is enticing. However, the physical realities associated with imaging in live tissue make this a continuously elusive objective, as will be evidenced in this review paper. Nevertheless, the information derived from in vivo fluorescence imaging systems can be regarded as an important complement to microscopy studies performed on cell cultures and tissue slices because it provides information about specific biological processes in fully integrated living systems[1]. Figure 1 illustrates the salient differences between in vitro, ex vivo and in vivo fluorescence from biological applications relating to brain imaging. Though in essence the underlying technological and biological principles appear to be the same, imaging in each of these regimes imposes unique challenges requiring significantly different approaches to system design.

In this review paper, the basic principles of imaging fluorescence in living tissue is described, together with the practical challenges in designing, implementing, and assessing these systems. Methods available to overcome some challenges using advanced imaging system designs are discussed and an appreciation of the importance and challenges relating to modeling light propagation in tissue is provided. Perhaps most important is to realize that there is an intrinsic limit on the biological information that can be extracted from even the most carefully designed in vivo imaging instrument. Understanding these limitations is critical for researchers in the biological sciences wanting to use custom or commercial in vivo systems in the scope of their research. If, at the onset of research planning, the intrinsic limitations do not interfere with investigational endpoints, a choice must be made among several technological offerings. This paper will help to guide these choices for systems currently available commercially and in research laboratories.

The paper is divided into several sections covering the fundamentals of fluorescence imaging through advanced technology topics. The *In Vivo Imaging Methods* section discusses the intrinsic limitations of whole-body imaging. These limitations relate to the interaction of light with microscopic tissue components as well as with the specificity and sensitivity of the contrast that can currently be generated in living animals. A description is also provided for the different types of imaging technologies that can be used for in vivo imaging emphasizing which biochemical fluorophore properties can be extracted from each. This is followed by a more detailed description of the various hardware components required in whole-body fluorescence imaging, including state-of-the-art illumination and light detection technology. This section concludes with a description of the various imaging geometries that can be used to perform in vivo small animal imaging. The next section, *Survey of Commercially Available Systems*, consists of an extensive survey of the main commercial systems available on the market. This is presented in parallel with a discussion of salient features of in vivo fluorescence imaging in terms of resolution, sensitivity and quantification. The section entitled *Applications* reviews recent publications where in vivo fluorescence imaging has been used to study certain biological phenomena. Finally, the paper concludes with a *Discussion* section reviewing the research done in laboratories to improve the capabilities of in vivo fluorescence imaging.

[1]In this paper the term *in vivo* is used in relation with studies performed using live animals, i.e., excluding work done with live cells in cultures (see Fig. 1).

2. In vivo Fluorescence Imaging Methods

2.1 Intrinsic limitations

In considering the potential use of in vivo fluorescence imaging in biological studies, there are intrinsic limitations researchers should probably consider. In part, these limitations relate to the interaction of light with microscopic components of tissue. Also, consideration must be given to difficulties insuring that biomarkers of interest are associated with a detectable level of optical contrast and that the origin of the latter is specific enough to deliver useful objective information.

2.1.1 Tissue absorption, scattering and autofluorescence—The basic principle behind in vivo fluorescence imaging is similar to that used in fluorescence microscopy techniques (e.g., conventional fluorescence microscopy, confocal microscopy, multiphoton microscopy, optical coherence tomography). However, when whole animals are interrogated, the desired information is typically associated with biochemical events occurring deep within the tissue. This implies that photons being part of the detected signal have undergone multiple scattering events in the process of irradiance of the excitation light into the body and radiance of the emission out of the body.

Microscopic components within tissue from small molecules (sugars, fatty acids, amino acids, nucleotides, ions, water) and macromolecules (proteins, phospholipids, RNA, DNA, polysaccharides) to larger structures such as organelles and cell membranes collectively absorb light in the ultraviolet (UV) through the visible (VIS) wavelength range, Absorption by tissue components in this wavelength range limits effective light penetration to a few hundred microns However, significantly larger depths can be probed using light in the far-red or near-infrared (NIR) wavelength range, where the main tissue absorbers are de-oxyhemoglobin, oxyhemoglobin, water and lipids. In this spectral region, the absorption of these chromophores is at least one order of magnitude lower than in the VIS part of the spectrum potentially allowing detectable signals to be measured through several centimeters of tissue.

In the NIR part of the electromagnetic spectrum, elastic scattering of photons dominates over absorption, making multiple scattering the main mechanism for light propagation. This phenomenon is so significant that on average photons have an equal probability of traveling in any direction after having penetrated less than 1 mm of tissue. One of the consequences of this is that light transport in tissue can often be modeled as a simple isotropic diffusive process with reasonable precision as soon as photons have traveled more than a few scattering distances [1]. This is a useful approximation because localization and characterization of diseased tissue beyond the surface becomes nearly intractable unless modeling techniques are applied to account for the photon scattering.

In the fluorescence process, scatter acts on both the excitation light and the fluorescence emission traveling back to the tissue detection area. This introduces an intrinsic blurring in fluorescence images, an effect that is amplified for fluorescent targets that are farther away from the illumination and detection area. Another important consequence of scatter is that it amplifies the effect of the wavelength-varying absorption spectrum of tissue chromophores, causing the shape and peak position of detected fluorescence spectra to vary depending on the pathlengths traversed by light in tissue [2].

Figure 2 demonstrates how photon scattering impacts fluorescence imaging in living tissue using two numerically simulated mouse models. An 8 mm diameter tumor was located in the abdomen in each simulated mouse, one near the surface and the other close to the axial center of the animal. A generic fluorescent probe was assumed to have been perfectly

absorbed by the synthetic lesion, providing an ideal though unrealistic infinite tumor-to-background contrast. The diffusion approximation to light transport was used to simulate the excitation light propagation into the tissue and the fluorescence emission, all from the top of the animal (epi-illumination mode) [3]. As is demonstrated in the figure, a tumor with the same contrast produces dramatically different intensities on the tissue surface depending on its depth. It should be noted that other factors such as imperfect filtering, non-specific probe fluorescence and tissue autofluorescence would yield even less accurate results. This demonstration simply illustrates how photon scattering manifests as one of the most significant difficulties in optical imaging of animals.

There is a wide variety of molecules present in living tissue that can act as biochemical sources of autofluorescence [4, 5]. Examples include tryptophan, NADH, pyridoxine, collagen, elastin, flavins, porphyrins as well as chlorophyll present in animal food. Because the main excitation peaks for the natural fluorophores are usually in the visible part of the spectrum, their impact on far-red and NIR fluorescence imaging is often negligible. Nonetheless, fluorescence signals from the molecular probe of interest can still be corrupted, especially when the probe is weakly fluorescing or sparsely distributed. For example, a weak autofluorescence signal from the skin can overwhelm the fluorescence from a deeply embedded tumor, and much of the autofluorescence in animals is located in the two largest organs, skin and colon. The autofluorescence from the food present in the colon can be minimized by feeding the animal with special non-fluorescent chow. The non-specific signal from autofluorescence can either mask desired signals or be erroneously attributed to the target signal, leading to an inability to discriminate the tissue of interest or to a severe overestimation of the probe's fluorescence activity. In recent years, careful implementation of time-resolved measurements or spectral unmixing techniques have been integrated into systems allowing correction for this unwanted signal [6, 7].

2.1.2 In vivo sources of optical contrast—Naturally occurring endogenous fluorescence from small animal tissue is not a source of contrast that is routinely used in the scope of preclinical studies, to a large extent because of the small contrast and specificity that is associated with it. Mainly, sources of fluorescence contrast in animal studies are from exogenously administered fluorophores, fluorophore precursors or genetic engineering to metabolically produce fluorescent proteins. In the case of exogenous or precursor fluorophores, the contrast between the targeted tissue and the normal tissue in live animals is orders of magnitude lower than what is demonstrated with the same probes in vitro, regardless of binding affinity or specificity. This is due to the presence of unbound fluorophore molecules and/or non-specific binding. Exceptions include tumor cell lines transfected with a fluorescent protein, such as some of the green or red fluorescence proteins (GFP, RFP), which are uniquely expressed in the cell types they are transfected into, thereby providing nearly perfect contrast. As with autofluorescence, weak signals from any fluorophore near the source or detector location can overwhelm the signals from deeper tissue regions under investigation. However, unlike autofluorescence, this signal is generated directly from the molecular probe itself. Therefore, using lifetime characteristics or spectral unmixing does not help decouple the fluorescence signal of interest from the nonspecific background signal. Interestingly, recent studies show that temporal techniques can help decouple these signals by exploiting different uptake and clearance characteristics specific to each organ [8].

The capabilities and limitations of all small animal fluorescence imaging systems can be understood in the context of these biophysical factors. Some of the challenges may be partially addressed through optimal hardware and software design, but some problems simply cannot be solved because of the intrinsic limitations described here, as will be evidenced in the remainder of the review paper.

2.2 Imaging fluorophore biochemical properties

The objective when designing a small animal fluorescence imaging system is the detection and mapping of specific fluorescent biomarkers relevant to the given biological study goals. By far, the most commonly imaged parameter is the intensity of the fluorescence emission, which is usually accomplished based on continuous-wave (CW) technology[2]. Usually, for relatively low fluorophore concentrations, the measured intensity is monotonically related to the product of the fluorophore concentration, the extinction coefficient and the quantum yield. However, in cases where the concentration is large, care must be used when interpreting fluorescent data because re-absorption of fluorescent light and quenching might impact the signal by making the emission process non-linear. Moreover, for tissue imaging the measured intensity emanating from sub-surface fluorophores depends non-linearly on the intensity of the excitation light because of scattering and absorption. This makes recovery of fluorophore biochemical properties, such as local concentration, reliant on light transport modeling as well as the experimental evaluation of intrinsic molecular parameters prior to in vivo imaging (e.g., quantum yield and extinction coefficient). Moreover, the ability to derive biochemical properties in vivo is in general reliant on carefully implemented calibration procedures that are unique for each imaging instrument.

Fluorophore concentration derived from fluorescent light intensity measurements is not the only property from which biological information can be obtained. Some systems are capable of imaging the fluorescence lifetime, revealing the influence of the chemical environment on the fluorescent molecules. An important aspect of lifetime imaging is that it is independent of fluorophore concentration and provides a method to explore tissue chemistry unique to fluorescence measurements. However, while fluorescence lifetime imaging has been demonstrated in live animals, extracting lifetime requires that measurements are resolved in time, increasing the complexity of the source and detector measurement system dramatically. This may be achieved either in the frequency domain (FD) or the time-domain (TD). In the case of FD technology, the excitation source is modulated with frequencies in the 100’s of MHz range and measurements consist in the phase shift of the time-varying fluorescence emission light. On the other hand, TD systems use pulsed sources and very sensitive gated detectors. Systems capable of these measurements (FD, TD) are described in more detail below. The frequency domain systems are not commonly used in small animal imaging, because the tissue thicknesses are small, and so the phase shift that would be measured would necessarily be low unless the frequency of operation was very high, i.e., above 300 MHz. As such, few systems have used this technology for small animal imaging because the cost is high and stability is lower than systems below this frequency range.

2.3 Instrumentation

The commercialization and development of prototype small animal fluorescence imaging systems has progressed rapidly over the past decade and a wide variety in approaches and components have been used. Optical devices are the highest growth area in pre-clinical imaging research and an increasing number of pharmaceutical companies use them in the development and assessment of new drugs. Others focus on the use of these instruments to follow longitudinal changes in diseased tissue in live animals, tracking disease progression or response to intervention. A review of commercial systems (see Section 3) reveals that the technology has not yet converged to a few widely applied technologies and that there exists a wide range of approaches and capabilities. The range of choices in the field is driven by factors such as cost, data types required, ease of use, ability to couple to other imaging systems, and scientific collaborations.

[2]In the biomedical optics literature, another word that is often used in place of *continuous-wave* is *steady-state*.

Figure 3 provides an overview of the hardware required for different types of imaging data. All in vivo fluorescence imaging systems are designed around the idea that a portion of the fluorescence emission spectrum of the molecule of interest can be separated spectrally from the excitation and/or background light signals. This is achieved with filtering strategies, such as dielectric interference filters, liquid crystal tunable filters, spectrograph gratings. Ultimately the filtering capability of a system is a major fundamental limitation which will dictate lower limits of detection of fluorophores.

For imaging applications based on cameras (see Figs. 4(a), (b), (d), (e) in the *Imaging geometries* section below), many filtering strategies such as interference filters can at best provide 2 to 3 orders of magnitude of suppression of the excitation light, and so the remainder of the excitation light is left to leak through to the detector and ultimately provides a background signal which must be accounted for. These attenuation factors are several orders of magnitude lower than typical values provided for high-end filters by manufacturers. Typically, the quoted values are for normal light incidence on the surface of the filters. However slight angular deviations from normal incidence lead to dramatic degradation of the attenuation power. For imaging applications based on cameras, the angle of incidence is not normal on average, which explains the relatively limited attenuation factors of these instruments. In situations where light is collected from a point or a small area on the surface (see Figs. 4(c) and (f) in the *Imaging geometries* section below), the filters can be placed in a near afocal geometry, allowing improved filtering of fluorescent light. Therefore, while filtering specifications are not commonly provided for a fixed source-geometry combination, this can be essential to evaluate for utility of the system.

When designing an imaging system, a reasonable strategy for maximizing signal intensity could consist in irradiating tissue with light such that the fluorescent molecules of interest are excited right at the peak wavelength of their absorption spectrum. However, the choice of the excitation wavelengths must be balanced with the ability of the detection system to filter or otherwise reject the excitation light in the measured signal. Consequently fluorophores with small Stoke's shifts, such as most organic fluorophores, are usually excited at wavelengths shorter than right on their absorption peak, in order to allow better wavelength separation between the incident light and the emitted light. Alternatively some fluorophores have multiple absorption bands allowing more flexibility when choosing the excitation wavelength. While some excitation sources allow flexibility in terms of illumination wavelengths, others are fixed and thus the fluorophores to be used must be considered in the design or purchase phase of the system.

Another factor to consider is the capability to use a priori knowledge of the spectrum or fluorescence lifetime associated with the detected light. Using grating-based spectrographs, liquid crystal tunable filters, or filter wheels with several bandpass filters over the emission range, pre-recorded basis spectra can be used to decouple the autofluorescence signal from the fluorescence of the probe. In addition to removing autofluorescence, spectrally resolved data can also provide a platform for imaging several fluorophores simultaneously, using the same spectral un-mixing algorithms, As seen in the *Discussion* section, this is a key feature of some of the more recently advanced systems available. Another method consists in using prior knowledge of the lifetime of the fluorophores to separate them based on time-resolved signals. Typically, this would involve fitting TD signals, obtained for example using time-correlated single photon counting technology (TCSPC), with multi-exponential expressions in order to determine the relative contribution of each major fluorophore. These techniques, either based on spectral signature or lifetime, have been used for planar and tomography imaging and can improve the sensitivity of the imaging system significantly. As seen in the *Discussion* section, this is a key feature of some of the more recently advanced systems available.

Excitation can be achieved by a wide variety of light sources including filtered filament or gas discharge lamps (tungsten and xenon), light-emitting-diodes (LED), or any laser system, including gas, crystal, and diode lasers. Versatile imaging instruments, in terms of number of available wavelengths, can be designed using expansive systems such as tunable lasers (e.g. Ti:Sapphire laser) but relatively inexpensive broad band lamps can be used to provide a flexible platform since filters can be used to select different excitation wavelengths. However, the isotropic emission of lamps limits the ability to focus a large amount of power on the tissue surface and limits their use to applications having large fiberoptic cable delivery or direct lens-based delivery of the light. Lamps also require relatively long warm-up times and are considerably less stable than solid-state devices. Intensity variations of lamps can be in the range of 10-50% over an imaging session, whereas the stability of diode lasers can typically be in 0.1% range if they are low power or temperature controlled. Finally, lamp-based systems are not suitable for time or frequency domain measurements which require precise and rapid modulation of the source intensity.

LED's and laser diodes (LD) are very stable and may be modulated or pulsed for time-resolved measurements. LD's are ideal for focusing power in raster-scanning or fiber-based light delivery geometries, though LED's may also be used if power requirements allow. Since LD's and LED's are available only for discrete or relatively narrow wavelength bands, systems capable of exciting fluorophores with different excitation wavelengths require multiple diode devices. This can increase the cost of the system, especially if power requirements require that diodes be cooled. Nonetheless many systems have gone to multiple bands of LEDs or LD's to provide the kind of flexibility now commonly available in flow cytometry. As mentioned above, tunable lasers provide the most flexibility in terms of wavelength, and can be operated in a pulsed mode, but are still comparatively expensive by almost an order of magnitude in cost. However certain systems, such as crystal lasers and Ti:sapphire systems and other options such as broad band supercontinuum laser sources, are increasingly becoming more reliable in their environmental controls and physical stabilization, as prices continue to notch downwards.

Available detectors also vary widely and include charged coupled device arrays (CCD's), intensified CCD's, electron multiplication CCD's (EMCCD), avalanche photodiodes (APD's), and photomultiplier tubes (PMT's). While the latter is by far the most sensitive instrument and offers exceptional dynamic range, the cost often prohibits use in parallelized high-resolution arrays. Furthermore, most PMT's lose sensitivity above 850 nm. PMT's are often used in scanning devices or fiber-coupled devices that acquire measurements sequentially. APD's cost less, but are also less sensitive than PMT's. CCD's are the most common among detectors and can image an entire animal with one acquisition. They are limited to CW measurements, though time gated operation is possible in some scenarios. Earlier and less expensive systems had 12-bit or 14-bit digitization in the acquisition providing a relatively limited dynamic range. Most current cameras operate with 16-bit digitization providing superior dynamic range because there the intensity range varies up to 65,536. Another important criterion here is that the number of bits available for digitization be matched with a chip having enough full-well capacity for the whole digitization range to be used. Large dynamical range can be especially important in background removal or for dealing with light leakage issues where image subtraction can effectively remove unwanted signals, and yet can easily preserve the key 8-bits (256 levels) of information that are displayed to the user. Since humans can only perceive about 8-bits of information, images are typically 'windowed' to the relevant 8-bits of display that preserves the minimum and maximum intensities in the image. Having a wider range of bits available in digitization allows better potential to accurately capture the relevant part of the signal, without having intensity saturation at the high end or all autofluorescence dominating at the low end of the intensity scale. The dark current of most imaging systems is not typically a major factor in

epi-illumination planar imaging, because the lower limits on detection are typically the autofluorescence of the tissue, and specular reflectance getting through the system filters. Thus, while bioluminescence or trans-illumination systems must have ultralow dark current levels that come with CCD's cooled to −90° C, the standard epi-fluorescence imaging typically does not.

2.4 Imaging geometries

Unlike x-ray imaging, which is always configured in simple planar-transmission geometry, the complicated nature of far-red and NIR light propagation in tissue makes the imaging configuration of fluorescence systems of critical importance, ultimately determining the information content of the images. Diagrams summarizing the various geometries used are provided in Fig. 4. In general, all measurements are acquired in either reflectance mode (henceforth referred to as epi-illumination), in which the source and detectors reside on the same side of the tissue (Figs. 4(a), (b) and (c)), or transmission mode (trans-illumination), which involves illuminating the tissue from one side and detecting the emitted light that has passed through the tissue (Figs. 4(d), (e) and (f)). Within these general categories, light sources and light detectors may be configured to achieve various spatial resolutions and enhanced tissue sampling capabilities.

Broad beam imagers use light sources spread over a large area, usually the entire animal. The emitted light is usually acquired over the entire illumination area through a camera lens/filter assembly attached to a CCD camera as shown in Fig. 4(a). While filtered lamps are commonly used for these systems, LED's and beam expanded lasers have also been used. Broad beam systems are simple, relatively inexpensive, and provide rapid acquisition since the entire animal, or a set of animals, can be imaged with a single exposure. These characteristics make the broad beam imaging systems attractive for many researchers. However, the simplicity imposes limitations on the information content extracted from the images. Specifically, broad beam systems are almost always configured in the epi-illumination geometry and are severely limited in their ability to probe deep tissues due to light scattering and non-specific signal contamination such as autofluorescence of tissue. As mentioned in the *Instrumentation* section, effective filtering of the excitation light is also a major issue in broad beam geometries because of angle of incidence related performance issues that are typical in all types of optical filters.

Some epi-illumination systems use raster-scanning devices for the source and/or the detector. Raster scanning sources are usually implemented with a collimated beam of light from a laser diode, redirected off of fast galvanometer scanning mirror units through a scan lens. Measurements can be made for each source position on the tissue surface through, for example, a telecentric scan system using two-axis galvanometer mirrors. Though not shown explicitly in Fig. 4, it should be noted that raster scanning illumination/detection could also be implemented using motorized fiber optic sub-assemblies. Some systems collect light from the entire tissue surface for each source position (Fig. 4(b)) while others may have a limited number of detector positions on the tissue surface for each source position (Fig. 4(c)). While different source-to-detector distances can be used to probe different tissue depths, even raster-scanning systems in the epi-illumination geometry suffer from relatively poor depth sensitivity and surface-weighted imaging.

Trans-illumination systems are configured such that the excitation and emission light is transmitted through a portion of the tissue, usually through the entire animal. By nature, the measurements contain information from deep inside the tissue, though each measurement represents an average of the tissue volume sampled by the bulk of the tissue through which the light has passed. If implemented in a broad beam planar imaging fashion, this type of imaging is akin to X-ray projection imaging methods similar to a mammogram technique

(Fig. 4(d)). Information can be extracted by calculating the ratio of the fluorescence and excitation intensities measured at the detectors which reduces the influence of varying optical properties in the tissue. Another possibility consists of incorporating tomographic image reconstruction techniques based on models of light propagation in tissue. These techniques are described in some details in the *Discussion* section.

Trans-illumination images contain more information and are more sensitive to deeply seated fluorophores than those acquired with epi-illumination configurations. Indeed, trans-illumination signals are only weakly affected by the depth of fluorophores while the corresponding signals in an epi-illumination system decrease exponentially with depth. While this is a clear advantage in terms of imaging accuracy, trans-illumination imaging is usually performed in a raster-scanning configuration (Fig. 4(e) and (f)) and therefore requires a substantially longer time to acquire a single image. This may be a significant issue if throughput is an important factor in the imaging study being performed. The reason trans-illumination is usually performed with lasers rather than lamps is that the path lengths that need to be traversed by light can be of the order of a several centimeters, therefore requiring relatively large energy deposition for scan times to be maintained to a reasonable level.

The configurations shown in Fig. 4 suggest that imaging is performed in planar mode with none of the main hardware components being allowed to move around the animal. However, although this is not shown in Fig. 4, the design of systems optimized for tomographic imaging is usually based on geometries in which the tissue is sampled in a manner more reminiscent of conventional x-ray computed tomography than to that of planar x-ray imaging. There are a wide variety of ways to achieve optical tomographic sampling of tissue, most of which involve the motion of sources and/or detectors around the animal.

3. Results: Survey of Commercially Available Systems

This section is focused on the general applications and performance issues relevant for researchers desiring to acquire or build a whole-body in vivo imaging system. As described earlier in this review, there is a variety of important factors that should be used to guide choices for in vivo imaging. The main categories for these factors are: (1) the targeted biological information, (2) the basic instrumentation and data types to be obtained, and (3) the imaging geometry. Specifically, this section discusses those aspects, using commercially available imaging systems to emphasize certain issues. The main types of applications are outlined as well as providing an assessment of the level of expectation a user should have in terms of system performance given the choice of the system.

3.1 Commercial whole-body preclinical imaging

As a basis for the discussion in this section, Table 1 summarizes the main technical features of the imagers that are commercially available, while Fig. 5 shows images acquired with each one of those eight systems illustrating specific features distinguishing the instruments,. It is clear that the information in Table 1 can become obsolete relatively quickly because of the possible commercialization of novel systems as well as the continuous upgrades that are being made on existing systems. However the aim here is to use the commercially available instruments as a technological baseline upon which the discussion of applications and performance issues can be made

Inspection of the summary table provides an overview of the main differences between the imaging systems. Most of the systems rely on illumination based on filtered lamps and detection based on a cooled CCD camera. The table provides the main technical specifications for each of these components. In the case of illumination, the type of lamp that is used is provided along with the maximum output power (all wavelengths combined).

In the case of CCD cameras, the cooling temperature is specified as a mean to assess the noise features of the chip. The resolution of the latter is also provided in terms of number of megapixels (MP) as well as the size of each pixel. Finally, when available the dynamical range of each CCD chip is provided in terms of the number of bits available. For three out of the eight systems, illumination is performed with laser diodes. For one of those systems, laser illumination is done at multiple points in order to generate trans-illumination CCD-based tomography datasets allowing fluorescence images to be reconstructed showing the distribution inside the body of the animal (Fig. 5(f)). One of the other laser-based systems uses sub-nanosecond pulsed laser diodes with PMT-based detection performed in conjunction with time-correlated single-photon counting technology (TCSPC). This epi-illumination system uses a raster-scanning method to sample areas of the animal surface. The time-domain nature of the signal allows the lifetime of the fluorophore (Fig. 5(g)) as well as its approximate depth to be extracted. The last laser-based system defocuses the light onto tissue in order to illuminate large areas. The collection is then performed with a CCD camera.

In the table, the applications each system is equipped to do are divided into six different categories, mentioned here in order of increasing data processing complexity: planar imaging, multiplexing, lifetime imaging, topography, spectral unmixing and tomography. Some important aspects relating to planar imaging, multiplexing and spectral unmixing are further described below, while lifetime imaging and tomography are addressed in the *Discussion* section.

3.1.1 Planar imaging—Planar imaging is by far the most common application and can be performed by all imagers found in the table. Scattered light propagation in tissue as well as the ubiquitous presence of autofluorescence in signals in general renders epi-illumination planar imaging sensitive to surface and, to a lesser extent, to subsurface fluorophores. The depth penetration increases for longer wavelengths. Also, the contamination with autofluorescence decreases for longer wavelengths, and is substantially lower once excitation is longer than 750 nm, i.e., in the NIR spectrum. The inherent impact of autofluorescence is intrinsically decreased in the case trans-illumination planar imaging, which can only be performed with a few of the commercial systems. Figure 5(e) shows two images of the same animal, one having been acquired in epi-illumination mode, while the other one has been acquired in trans-illumination. Most of the fluorescence contrast in the epi-illumination image comes from autofluorescence, which is mostly absent on the trans-illumination image.

3.1.2 Multiplexing—The pool of potential fluorophores that can be used in the scope of preclinical studies is vast [9, 10]. Since each of these fluorophores have different excitation and emission properties (peak position, spectral shape), an important property that a system should have is versatility in terms of potential excitation and emission wavelengths that can be isolated with the use of filtering techniques. Systems that are based on lamps are inherently more flexible in terms of available excitation wavelengths when compared with laser-based systems which would require several laser diodes to be used. In terms of light collection, both CCD-based and PMT-based systems come equipped with a mechanism for filtering the light. The intrinsic spectral sensitivity of the CCD chip as well as the PMT is important in determining the versatility of a system, as well as the number of motorized filters that can be installed in front of the detector and used for imaging the same animal. This is relevant when multiplexed images need to be acquired to highlight different fluorophores almost simultaneously. Figures 5(a), (b) and (c) show planar epi-illumination images corresponding to single-wavelength, dual-wavelength and tripe-wavelength multiplexed images, respectively.

3.1.3 Spectral processing to identify fluorophore signals—The most versatile system in terms of multi-spectral imaging is that which is equipped with liquid crystal tunable filters. This technology allows for the isolation of specific spectral bandwidths with a choice of resolutions down to a few nanometers. The acquisition of a 'spectral cube' of data allows the data processing to go one step further than in the case of multiplexing. In fact, state-of-the-art algorithms have been developed which are able to isolate the contribution of individual fluorophores, including the contribution of autofluorescence. This feature is particularly useful for sub-surface imaging where autofluorescence is known to often contribute a great deal. Routine use of this type of algorithm requires the user to define databases of basis in vivo fluorophore spectra against which the data cube is fitted.

Other technical instrument features represented in Table 1 are related to how they facilitate the experimental workflow of preparing and imaging animals. This includes such things as the presence of hook-up for anesthesia tube, temperature controlled animal environment as well as the number of animals that can be imaged simultaneously. Other parameters of importance are related to multi-modality imaging. This can take multiple forms, the most basic of which being the availability of a white-light imaging system showing the user a visible image overlaid with a fluorescence image. This, or the presence of a profilometry system, can be used to provide a minimal anatomical reference against which one can interpret the spatial location of the imaged fluorescent sources, as is seen in Fig. 5. Other more sophisticated ways to provide anatomical landmarks consists in coupling the imager with a structural modality such as a planar x-ray system (Fig. 5(h)). The multi-modality imaging section in the table also provides information about the extent of which the instruments come equipped with tools facilitating the co-registration with images acquired with different modalities. This comes either in the form of multi-modal mouse beds accompanied with image fusion software or simply in the form of registration software based on optical fiducial mapping.

3.2 Performance requirements

To this point, both in the research community (see *Discussion* section below) as well as in the commercial world, the range of uses required is not realistically contained in a single instrument, typically because of patent niches, markets and costs limitations. Therefore, prior to building or acquiring an imager, it is important to decide what type of biological question the instrument is expected to help answer. A feature that makes the field of in vivo imaging challenging for medical imaging scientists but perhaps daunting for users, is that no clear consensus has been reached determining the limits of the approach and the optimal configuration, in terms of hardware, software and data processing methods. In fact, as will be shown in the *Discussion* section, there is still a large community of scientists working on different fundamental aspects of whole-body in vivo fluorescence imaging. Still, there are certain features of the modality which cannot be circumvented no matter how well an instrument is designed with the existing technology. These limitations, further described below, broadly fall into three categories, namely: spatial resolution, sensitivity, and quantification. It should be mentioned that prior to acquiring an in vivo imager, the manufacturer should be able to provide clear guidelines mapping those limitations onto the biological questions one is interested to investigate.

3.2.1 Spatial resolution—In mice, the spatial resolution of the imaging approach is fundamentally limited by the scattering nature of light, and this can vary between different systems and methods as well as between different biological applications. The most dominant and perhaps least commonly understood part of optical imaging is the fact the spatial resolution of planar images will vary considerably with depth of the fluorophore distribution, thereby making interpretation of the images reliant on a proper appreciation of

light transport in tissue. The spatial resolution can be as good a microscopy (i.e., a few hundred microns) on the surface of tissue if the system is designed that way, but degrades considerably with depth, reaching perhaps less than one millimeter for sub-dermal imaging in broad beam epi-illumination mode, and degrading to a few millimeters at depths in the middle of a mouse. This depth-dependent resolution is a ubiquitous trait of epi-illumination imaging, the impact of which is slightly reduced if planar imaging is performed in trans-illumination mode. Systems relying on imaging methods appropriate for fluorescence tomography can partially avoid this pitfall because light-transport models are then used as part of the reconstruction method aiming at recovering the position of the molecules. Again, this increased precision comes at the cost of increased imaging times as well as potential problems created by the increased complexity of the image reconstruction method. Raster-scanning approaches can lead to improved quantification and resolution for surface imaging [11], but actually are less efficient at detecting deeply seated fluorophores, unless the source and detector fibers are separated spatially. However, raster scanning also comes at the cost of a significantly increased imaging time that decreases animal throughput, which can be detrimental to the conduct of large volume preclinical studies.

3.2.2 Sensitivity—Sensitivity refers to the concentration or density of fluorescent molecules that can be locally detected in an animal. The signal emanating from the target is always polluted by non-specific signals coming from autofluorescence of tissue, excitation light leakage through the filters, as well as biological signals in the form of unbound exogenous dyes or contrast agents present in the blood or organs which are not relevant to the study design. Typically, a large part of the autofluorescence comes from the skin while the non-bound or non-specifically bound components can potentially come from anywhere within the animal. This implies that for an imager to be efficient, the detection system should have acceptable noise characteristics, but more importantly large dynamic range to allow background removal techniques to be applied to the signal. If the dynamic range is too small, it is likely that in applications where targets are associated with smaller contrast than autofluorescence will dominate the detectable image. At a minimum, an in vivo system should come equipped with a cooled CCD camera with large dynamic range. Some systems allow for the possibility to perform bioluminescence imaging. In this case, there is no autofluorescence but signal levels are typically two to three orders of magnitude smaller than for fluorescence imaging. Ideally these systems must use CCD cameras cooled down to −90°C or internal gain detectors (e.g., EMCCD, PMT). This level of noise suppression is not really necessary for epi-illumination imaging but in some instances can be useful for planar trans-illumination and tomography because of the reduced signal that is acquired.

3.2.3 Quantification—Quantification refers to the potential of an instrument to provide data sets from which the correct concentration or density of molecules can be retrieved. In its current implementation (commercial and laboratory systems), in vivo fluorescence imaging is not a modality that is capable of providing quantitative information in the strictest sense of the term. In principle, quantification in fluorescence imaging can be approached only through a combination of light transport modeling, data normalization and calibration. The closest to actual quantification that optical fluorescence sampling has achieved is through the use of normalized datasets, either in the ratio of emission to excitation [12, 13], or in the wavelength ratio of the fluorophore at different wavelengths [14]. Ref. [13] has shown that the approach of normalized emission/excitation ratio for fluorescence tomography works well, because the signals have travelled more or less the same tissue pathlengths. The impact of this normalization is to approximately cancel out geometrical and heterogeneity effects that cannot be controlled experimentally, because they enter the signal typically as multiplicative factors, and are roughly equal in magnitude for each of the two signals. Similar normalization or ratiometric approaches can be achieved

with two wavelength approaches in either excitation or emission, yet a hard comparison of signal to noise with these techniques has not been established. This approach is very important because of the complex shapes and highly heterogeneous optical properties of small animals in vivo, which are difficult to control for or accurately model with light transport tools.

Spatial resolution, sensitivity and quantification potential are features that a manufacturer should be able to provide a user prior to acquiring an instrument. Beyond this, commercial systems are used in research laboratories for a variety of applications, a review of which is provided in the next section. Analysis of these applications shows that biological studies are concerned with certain traits which are commonly required from an instrument. Below, an enumeration of these traits is accompanied by the main system characteristics that are facilitating them.

- **Detection of deeply seated fluorophores:** planar trans-illumination imaging (Fig. 5(e)), fluorescence tomography (Fig. 5(f)).
- Discrimination between specific and non-specific fluorescence: spectral unmixing (Fig. 5(d)), lifetime imaging (Fig. 5(g)), multiplexing (Fig. 5(b) and (c)), kinetic imaging methods [15].
- **Large animal throughput for accelerated research:** epi-illumination CCD-based imaging coupled with optical lenses conferring large field-of-view.
- **Localization of fluorescent molecules in 3D:** fluorescence tomography (Fig. 5(f)) and topography.
- **Co-registration with anatomic landmarks:** integrated structural imaging modality (Fig. 5(h)), animal beds compatible with magnetic resonance imaging (MRI) or computed tomography (CT), co-registration software based on optical fiducials or profilometry image (see, e.g., [16]).

4. Applications

Whole-animal fluorescence imaging has found widespread use in preclinical studies of disease progression and pathology, response to therapy, receptor targeted applications and probe development. An organ system overview of recent developments and applications of in vivo whole-body fluorescence imaging is presented below.

4.1 Neurological

At the level of the nervous system, the various in vivo fluorescence imaging techniques have been mostly exploited to image brain tumors in mice [17-20]. MRI co-registered fluorescence tomography (FT) was used to quantify cathepsin B activity in glioma tumors and monitor chemotherapeutic response to temozolomide treatment [17, 18]. There is also evidence of improved detection of diffuse gliomas using a EGF-targeted dye when compared to the gold standard of MRI [19]. Veiseh et al. used Cy5.5-conjugated chlorotoxin to image malignant gliomas and medulloblastoma brain tumors with exquisite resolution of cancer foci from normal tissues without the need of an impaired blood brain barrier (BBB) [20].

In addition to mice tumor models, fluorescence imaging has been exploited to further understand epilepsy, dementia, stroke, drug delivery, and BBB changes. Semi-quantitative planar fluorescence imaging and CT-coupled FT using a fluorescent probe that binds amyloid-β plaques probed burden of disease in an Alzheimer's disease mouse model [21, 22]. In a different application, diffuse optical tomography (DOT) was used to study the course of epileptic seizures and subsequent localization of epileptic foci [23]. In a mouse

model of cerebral infract, planar fluorescence imaging and a new albumin-conjugated dye were used to longitudinally monitor BBB impairment following arterial occlusion [24]. In another study, they showed increased levels of fluorescence due to anti-CD40 antibody accumulation in the stroke-affected hemisphere [25].

Matrix metalloproteinases (MMPs) appear to be implicated in the pathophysiology of stroke. Using their animal model of cerebral infract, Klohs et al. studied MMP activation using an MMP-activatable probe, and showed significantly higher levels of fluorescence in the stroke-affected hemisphere. Furthermore, they also showed a significant decrease in fluorescence and lesion volumes with administration of MMP inhibitor [26]. Johnson et al. showed that intrathecal delivery of butyrylcholinesterase led to visualization and quantification of drug distribution to the central nervous system [27].

Using planar fluorescence imaging, Pham et. al. assessed a newly synthesized cargo moiety for delivery of imaging or therapeutic agents due to its ability to cross an intact BBB [28]. Some of these studies provide the advantage of in vivo, noninvasive, and longitudinal imaging of fluorescent agents across the BBB, in sharp contrast to standard ways of assessing BBB passage, i.e., ex vivo visualization of Evans Blue accumulation in the brain. To date, whole-animal fluorescence imaging has shown promise in understanding brain physiology and pathology in a broad range of circumstances from cancer, to epilepsy, to BBB physiology, and targeted probes in a non-invasive and longitudinal manner.

4.2 Cardiovascular

One of the most significant pathogenic processes in cardiovascular disease is atherosclerosis, which causes vasculature plaque formation, and, when severe enough, can lead to tissue infarction and death, e.g., heart attacks, or myocardial infarcts. By taking advantage of in vivo fluorescence imaging capabilities, researchers have been able to probe at these two pathological states: atherosclerosis [29-31] and myocardial infarction [31, 32].

Many factors are involved in the pathogenesis of atherosclerosis, but macrophages are known to be involved in the formation and associated complications of atherosclerotic plaques, e.g., plaque ruptures with thrombotic events. FT on atherosclerotic mice visualized fluorescent signals from matrix metalloproteinase and cathepsin B activatable probes that co-localized to atherosclerotic areas of macrophage infiltration [29-31]. Planar fluorescence epi-illumination imaging was used to image hypochlorous generating MPO positive cells as a means to detect atherosclerotic plaques [33]. These studies provide evidence regarding the usefulness of this imaging modality to study atherosclerosis and basic molecular and cellular inflammatory processes (e.g., HOCl production and phagocytic activity).

In a mouse model of infarction, FT visualized phagocytic protease activity and macrophage magneto-fluorescent nanoparticle uptake in wild-type and wound-healing deficient mice. This study found that nanoparticle and protease-activatable fluorescent probe co-localized with MRI, histological, and immunohistochemical areas of tumor infarct and macrophage infiltration [34, 35]. This work has shown how FT may be used to non-invasively characterize the progression of healing in a myocardial infarction. All these applications have taken advantage of known biological processes specific for the disease in question (i.e., protease activity in macrophages, and developed fluorescent-targeted probes to quantify those processes).

4.3 Respiratory

To date, efforts using optical imaging of the respiratory system have focused primarily on lung tumor imaging [36-39] and airway inflammation [37]. A tomography system was used to image a mouse lung tumor model in which fluorescent yields were reliably used to assess

disease progression [39]. Another use of in vivo tomography imaging probed gene expression profiling of proteases in lung cancer. A strong correlation between tumor size and fluorescent signal in an animal model of primary lung adenocarcinoma was found using a protease-activatable probe with CT coupled FT [40].

Using a fluorescent protease-activatable probe and a fluorescent intravascular probe in FT, a murine model after lipopolysaccharide (LPS)-induced airway inflammation showed co-localization of fluorescent signals to areas of inflammation and LPS passage. In addition, a linear, dose-dependent trend in LPS dosage and protease activity was noted [37]. In a mouse model of eosinophilic-induced airway inflammation, FT detected eosinophil-specific probe activity to lower airways and lung parenchyma as well as response to dexamethasone treatment [41]. These reports showed the feasibility of using FT for in vivo study of the time-dependency of inflammatory insults to the respiratory system.

4.4 Gastrointestinal

Fluorescence imaging of whole-animals at the gastrointestinal level has focused mostly on developing betters ways to image, quantify, and monitor neoplastic disease. Montet et al used FT to quantify the vascular volume fraction (VVF) in an orthotopic colon cancer model and an ectopic tumor model. Investigators were able to monitor the course of angiogenesis and therapeutic response to anti-angiogenic treatment [42]. Von Burstin et al probed the sensitivity limits of their fluorescence system to detect early pancreatic cancer using two different protease-activatable NIR fluorescent probes: one to cathepsin B/H/L/S proteases and the other to matrix metalloproteinase. Both NIR fluorescent probes were detected at the earlier stages of disease [43]. An orthotopic RFP-expressing pancreatic cancer model was assessed for tumor burden and progression, with a high correlation in tumor burden found between fluorescence and ultrasound imaging [44]. In a similar study with a GFP-expressing cell line, Wack et al. detected pancreatic cancer with exquisite specificity and sensitivity [45]. Studies combining fluorescence tomography with MRI have shown that EGF uptake could be tracked in pancreatic tumors over time, where tumor size was imaged with T1 and T2 MR, and EGF signals were sampled by injection of EGF-IRDye800CW [46].

4.5 Immunological

One developing application of whole-body fluorescence imaging has been in lymphangiographic fluorescent methods to image lymphatic vessels, drainage, and sentinel nodes [47-50]. In a study using planar epi-illumination imaging, lymphatic vessels and their axillary lymph node sites of drainage were visualized using a NIR quantum dot probe [49]. The same research group developed a multicolored, lymphangiographic method with cyanine dye-conjugated immunoglobulins to map the lymphatic drainage patterns into corresponding axillary, cervical and thoracic nodes [48]. Mapping of lymphatic drainage and lymph nodes was also done using dual-modality, radionuclide-coupled fluorescent probes [47] or to Gd(III) for MRI [50].

In a study using FT, Garofalakis et al. identified GFP expressing T cells in mice with limits of detection as low as 3×10^5 T cells in the spleen and thymus [51]. The effects on T cell accumulation and their longitudinal changes in lymphoid organs was measured with FT in transgenic mice with GFP-expressing T cells following brain ischemia [52]. In another study, FT detected fluorescent-labeled cytotoxic T lymphocytes (CTLs) to monitor CTL immunotherapy and biodistribution [53].

The immune system plays an essential role in rejection of transplanted organs. Recently, Christen et al. used FT to detect and monitor macrophage response in heterotropic cardiac isografts and allografts. They were able to quantify differences in rejection between the two

types of grafts using fluorescence imaging [54]. FT holds promise in providing a quantifiable in vivo imaging modality to track various cell-specific processes of the immune system, such as macrophage recruitment, T cell distribution, non-specific phagocytic activity, and transplanted organ rejection.

4.6 Musculoskeletal

Musculoskeletal processes such as bone formation, resorption, and quiescent bone maintenance require a balance between osteoclast and osteoblast function. Current attempts in visualizing the musculoskeletal system have taken advantage of basic features inherent to these processes [55-58]. In one study, FT was used to image the complete growing skeleton and corresponding osteoblastic activity with a bisphosphonate-conjugated NIR fluorescent probe with high binding affinity to hydroxyapatite, the major mineral product of osteoblasts and other calcifying cells. Furthermore, FT compared to 99mTc-MDP radioscintigraphy showed better resolution of anatomical structures, faster acquisition times, but poorer visualization of deep tissues [56]. In a similar study, active bone formation and bone resorption as well as quiescent bone using FT imaged a neonatal, adult mouse with bone defects [55]. MicroCT and FT quantified two different dimensions of bone formation in mice following implantation of mesenchymal stem cells over-expressing the osteogenic gene, BMP2 [58]. A cathepsin protease-activatable probe measured osteoclast activity and detected bone loss 6 days before conventional radiographic techniques in an ovariectomized mouse model, i.e., a mouse model to monitor bone loss as a result of estrogen removal [59].

FT with a bisphosphonate-conjugated NIR fluorescent probe imaged regions of bone formation, but, like 99mTc-MDP, was unable to visualize osteoclastic surfaces from osteolytic metastasis [55]. In vivo fluorescence imaging was used to detect the specific bony biodistribution of multiple myeloma lesions manifested in diffuse bone disease - a hallmark of multiple myeloma metastatic cancer [60]. Fluorescence imaging of a GFP-expressing prostate cancer bone metastasis mouse model detected early intraosseous tumor growth [61]. Fournier et al. used a GFP-expressing breast cancer bone metastasis mouse model to measure tumor burden and assess the effects of bisphosphonates on osteolysis and tumor growth [62].

In addition to studying bony processes, some manifestations of autoimmune disease, such as rheumatoid arthritis (RA), are a common ailment affecting the musculoskeletal system. In an RA mouse model, FT localized fluorescence in arthritic joints from protease-activatable probes, and subsequently, monitored therapeutic response to the immunosupressant drug methotrexate [63]. Since evidence shows that activated synovial macrophages express a particular kind of folate receptor, a folate-linked NIR fluorescent probe was used for early and late in vivo detection of arthritis in two different animal models [64]. In vivo fluorescence imaging also assessed response to arthritic treatment. IKK-2 is a potent inhibitor of NF-κB, known to play an important role in arthritis. In an arthritic animal model where higher levels of fluorescence at arthritic joints correlate with extent of disease, IKK-2 treated and control animals displayed similar (lower) levels of fluorescence. Meanwhile, arthritic animals that did not undergo treatment had significantly higher levels of fluorescence [65].

4.7 Reproductive

Most of the work to date using whole-body fluorescence imaging of the reproductive system has focused on ex vivo fluorescence imaging of ovarian peritoneal metastatic models [66-72]. These studies developed ovarian peritoneal metastatic models, injected a targeted fluorescent dye, sacrificed the animals, and subsequently used whole-body fluorescence imaging. Investigated targeted probes include: D-galactose receptor ligands [66, 69, 72],

lectin-binding BODIPY conjugated avidin dyes [67], a dual modality MRI-fluorescence dye [68], a β-galactosidase activatable probe [71], and a self-quenched avidin dye [70].

4.8 Targeted probe development

To date, development of diagnostic or therapeutic targeted probes remains the most common application of whole-body fluorescence imaging. These probes have been used to study vascular endothelial growth factor [73], endothelial cells [74], acidic pH-activatable environments [36], integrin proteins key in angiogenesis of tumor vasculature [75], blood-pooling agents [76], NIR fluorescent probes for dynamic contrast enhancement [15, 77], fluorescent-protein expressing tumors [78-80], transgene expression [81], receptor targeted probes [82, 83], quantum dots [83-85], apoptosis detection [86], and metalloexopeptidase involved in cancer pathogenesis [87], among others. One major application of in vivo fluorescence imaging has been to use fluorescent-tagged antibodies to detect tumors over-expressing receptors of interest. Two studies localized and differentiated subcutaneous tumors with different levels of receptor over-expression: (1) tumors over-expressing EGF receptors, HER1 or HER2; (2) tumors over-expressing interleukin receptor, IL-2Rα; and (3) control tumors without over-expression of a targeted receptor. Tumors were simultaneously visualized and differentiated in the same animal using a cocktail of fluorescent-tagged antibodies [88, 89]. Gee et al. distinguished tumors over-expressing different levels of HER2, and subsequently monitored response to treatment with the HER2 antibody, trastuzumab [90].

MMP is involved in tumor infiltration and aggressiveness. With the use of an MMP-activatable probe, Bremer et al. detected MMP-over-expressing subcutaneous tumors [91]. A multimodal contrast agent, gadophorin, was used to study the organ-specific biodistribution of hematopoetic cells using MRI, in vivo fluorescence imaging, and fluorescence microscopy [92]. Carcinoembryogenic antigen (CEA) is a well-studied marker for various tumors, and recently, fluorescence imaging in vivo was used to detect CEA-over-expressing tumors with a new, high-afinity anti-CEA probe [93].

Asialoglycoprotein receptor (ASGP-R), a radioscintigrapic 99mTc-labeled pharmaceutical target, was recently visualized with a NIRF-DTPA-galactosyl-dextran ligand [82]. A fluorescent caspase-activatable apoptosis-specific probe detected in vivo parasitic induced apoptosis in liver abscess and colon xenograft mouse models [86]. Duysen and Lockdridge used whole-body fluorescence imaging to study the activity, biodistribution, retention, and clearance of the organophosphate bioscavenger, butyrylcholinesterase [94].

In addition to receptor-targeted applications, Yang et al. used a GFP-expressing adenoviral vector to monitor transgene expression in multiple organs using a planar epi-illumination fluorescence imaging system [81]. Dynamic contrast-enhanced fluorescence imaging simultaneously tracked the pharmacokinetics of two different fluorescent-tagged proteins [77]. Hillman et al. developed a technique called dynamic fluorescence molecular imaging whereby they study a dye's in vivo biodistribution dynamics to develop anatomical maps for organ identification and delineation [15]. A mouse model of adoptive transfer using a Matrigel matrix implant with or without seeded human endothelial cells was distinguished in vivo using a Cy5.5-anti-CD31 (anti-endothelial) antibody [74]. Another probe undergoing pH-specific activation in lysosomes selectively tagged viable tumor cells in vivo [36].

Studying tumor vasculature and angiogenesis is an important application to whole-body in vivo fluorescence imaging [42, 75, 76]. Tumor vasculature differs from normal vasculature in many respects, including disordered vasculature, increased leakiness, deficient endothelial junctions, and over-expression of particular receptors. Chang et. al. developed a fluorescence imaging strategy to monitor levels of vascular endothelial growth factor

(VEGF) in various tumors as well as monitor changes in VEGF expression following antibody [95] or photodynamic therapy (PDT) treatment [73]. A perfusion type optical contrast agent, SIDAG, was used to investigate the degree of angiogenesis, with results showing a strong correlation with angiogenic burden [96]. In a similar study, Montet et. al. quantified the vascular volume fraction of tumors with FT as a measure of angiogenic burden, and subsequently monitored response to anti-angiogenic treatment [97]. FT quantified and distinguished between three tumors with varying expression levels of the proliferating endothelial $\alpha_v\beta_3$ integrin receptor [98]. Cai et al. used a peptide labeled quantum dot that specifically binds to $\alpha_v\beta_3$ integrin receptor in vivo [75], and another report detected tumor vasculature by a multispectral unmixing technique in a RFP-expressing tumor [76].

5. Discussion

Whole-body in vivo fluorescence imaging is evolving, and may likely never reach a steady state, as the applications and technological opportunities continue to drive this evolution. There is a dynamic community of scientists involved in development of innovative approaches to improve and characterize these modalities beyond what has been achieved thus far, and as discoveries are made, the equipment and applications will advance. This research is pursued with the goal of understanding and minimizing the impact of the intrinsic limitations of the systems reviewed in this paper. A crucial part of the research that is conducted consists in the development of novel molecular imaging probes that can highlight more specifically biomarkers of disease [99-101]. Significant work is also devoted to the development of novel fluorescent proteins with spectral features allowing them to be used for deep tissue imaging [102-105]. Providing a review of in vivo fluorescence contrast agents and the relevant biochemical mechanisms is outside the scope of this paper. Instead, this discussion section provides an overview of the current work that is performed in research laboratories aiming at improving the performance of whole-body fluorescence imaging.

As seen in this paper, the preclinical work based on diffuse optical fluorescence imaging is to a large extent done through planar epi-illumination imaging. Although this is not the direction into which most innovative research and development efforts are concentrated, innovative work has been presented improving the performance of epi-illumination imaging. One such line of research consists in recovering planar images in terms of fluorophore lifetime. For example, Hasan et al. [106] and Bloch et al. [107] present methods to recover lifetime images based on time-domain technology. Meanwhile, the work of Hutchinson et al. [108], Kuwana et al. [109] and Hattery et al. [110] is concerned with lifetime imaging based on frequency-domain data sets. However, an important part of the research conducted in whole-body small animal imaging is concerned with the development of novel fluorescence tomography approaches pushing further the limits of the modality in terms of sensitivity, quantification and spatial resolution. This research can be divided in several non-exclusive areas from the design of state-of-the-art instruments to the development of sophisticated data processing algorithms and software.

5.1 ‘State-of-the-Art’ fluorescence tomography instruments and methods

The drive to realize full 3D optical capabilities has been a technological challenge that many researchers have investigated, with varying levels of success. The fluorescence tomography problem is a difficult one to resolve because of its hyper-sensitivity to various sources of noise such as modeling errors and statistical noise. In part, this is caused by the fact that the diffuse optical tomography problem is intrinsically ill-posed meaning that for a given fluorescence dataset there exists a large number of equivalent solutions. The challenge of researchers working in this field consists of devising approaches that minimize this effect,

ensuring that the images that are obtained are as close as possible to reality. There are several approaches to this problem, with perhaps the most brute-force one being using datasets consisting of a very large number of measurements in a manner that maximizes the amount of tissue that is sampled. Another approach consists of redefining the tomography problem in such a way as to provide prior spatial information based on structural images for the location of the expected source of fluorescence. This latter approach brings together the strengths of optical spectroscopy and avoids the weakness of poor spatial resolution, by using structural imaging of other highly-resolved modalities such as CT, MRI or ultrasound. The advent of spatially-guided fluorescence tomography represents a major paradigm shift in the development of fluorescence imagers. Admittedly though this shifts the costs structure of optical imaging significantly, as it ties it to availability of these more expensive imaging systems. Coupling to ultrasound may prove more economical for applications where this imaging helps visualize regions, as shown in Gruber et al. [111]. Other tomography approaches include using data types in the reconstruction process that are more strongly dependent on fluorophore properties, such as multi-spectral or time-resolved data sets.

Early fluorescence tomography instruments that were introduced are stand-alone in the sense that the information they provide is strictly in the form of functional or molecular images of specific biomarkers without structural landmarks. In most cases the outer surface was extracted by an external mean such as laser profilometry or stereo-vision as is required for modeling light-transport. A notable exception consisted in a system where the animal was immersed in an optical matching liquid with properties resembling those of tissue [112]. At the time, this approach was deemed acceptable because of the relaxed requirement for extracting the surface boundary for light transport modeling. However, matching liquid-based approaches were mostly abandoned due to cumbersome nature of the animal preparation process, which was significantly slowing down preclinical studies as well as limiting biological applications to organs below the neck. Other single-wavelength stand-alone systems based on CCD detection and CW technology were also developed (see, for example, Refs. [113-116]). The imaging geometry of these systems is such that large measurement densities are acquired in trans-illumination mode. Another generation of systems was developed with richer information content in the form of multi-spectral data, either at the level of the excitation or emission wavelengths. For example, Davis et al. [117] introduced a fiber-coupled CCD-based multi-spectral emission system using frequency-domain technology, while the multi-spectral systems introduced by Zavattini et al. [118], Leavesley et al. [119] and Li et al. [120] showed non-contact CCD-based instruments relying on CW technology. The tomography systems presented by Kepshire et al. [121], Brambilla et al. [122], Kumar et al. [123] and Niedre et al. [124] are different in the sense that they are based on time-domain detection, either through the use of gated CCD cameras or time-correlated single photon counting technology. Time-resolved imaging increases the information content of the signal by, for example, allowing researchers to study lifetime variations induced by different biochemical environments.. Another advantage of using time-resolved systems is that datatypes such as mean time of photon arrival and time-gated signals can be used potentially leading to improvements in the precision of recovered 3D fluorescence images (see, e.g., the work of Lam et al. [125], Riley et al. [126], Niedre et al. [124] and Leblond et al. [127]). The tomography systems mentioned thus far in this section all acquire data in trans-illumination mode. However, the work of Kepshire et al. [128] presents the development of a CCD-based epi-illumination CW raster-scanned tomography system. It was found that this geometry severely limits the potential to perform tomography to a depth of about 20 mm for spatial localization with, however, quantification capabilities exponentially decreasing with depth.

In parallel with the development of innovative imaging methods, data processing algorithms and software are being developed with the aim of maximizing the amount and the precision

of biological information that can ultimately be extracted from in vivo datasets. In particular, Refs. [13, 95, 129-157] develop approaches improving the methods used to solve the fluorescence tomography problem based either on single-wavelength continuous-wave or frequency-domain datasets. Then, Refs. [158-160] introduce algorithms for multi-spectral image reconstruction providing evidence that the quality of reconstructed images can potentially be improved with this approach. References [125, 126, 161] provide indirect evidence that imaging gains can be obtained from tomography datasets acquired with time-domain technology [125, 126]. Approaches using specific features of time-domain have also been developed showing promise for improving upon the main limitations of in vivo fluorescence imaging. Refs. [129, 143, 162-172] present the development of image reconstruction methods, showing that it is possible to image lifetime in small animals from deeply seated fluorophores. References [124, 127] show how using light signals from photons that are weakly scattered can significantly improve the resolution of fluorescence tomography.

As mentioned previously, significant research effort is invested in building systems that are combining fluorescence imaging with modalities providing high spatial resolution structural information. An example of this is the instrument presented in Davis et al. [117] where fiber-based optical detection is performed within the core of a 4T MRI system. In multi-modal approaches such as this one, the structural information is used in different ways. The simplest one consists in overlaying the fluorescence tomography images on the structural image allowing the localization of the fluorescent sources against anatomical landmarks [113, 121]. A more involved technique consists in using the anatomical information to impose constraints when resolving the fluorescence tomography problem thereby potentially improving the accuracy of the reconstructed images. In some cases the biological target of interest (e.g., a tumor) can be seen in the anatomical images. Then, this spatial information is used to guide convergence of the reconstruction algorithm toward those solutions that are consistent with the location of the sources of fluorescence. References [7, 21, 117, 121, 173-177] present data processing methods and analysis showing that the inclusion of prior structural information can in fact improve the accuracy of fluorescence tomography images.

5.2 Technology assessment

The main thrust of this review paper has been the presentation of current and prospective technology that can be used to perform whole-body in vivo fluorescence imaging. Emphasis has been on aspects such as intrinsic limitations and potential uses of the modality, instrumentation components, advantages and disadvantages of different imaging geometries, characterization of available commercial systems, and, finally, a review of the literature presenting biological results derived from this multi-faceted approach. In retrospect, it is apparent that the full potential of in vivo fluorescence imaging has not been fully exploited yet. The wide variety of available commercial systems (Table 1) partly illustrates this fact demonstrating that a clear consensus may never emerge as to the optimal approach for in vivo small animal imaging. This is because the choice of any one individual system is associated with one offering a balance between sufficient biological information at a price compatible with the scale of the available funding or related to the cost-effectiveness motive of the user. There will always be a tradeoff between financial investment for biological information that will provide a range of quality in the systems, as is true with standard human imaging systems as well.

Leaving aside issues relating to development costs, an important aspect that has to be considered in assessing the state of the technology is that convergence to a universally adopted imaging method is prevented by the wide variety of biological markers and fluorescent probe combinations that are being used and that will be developed for future preclinical applications. Each biological application typically involves fluorophores with

different spectral signatures, anatomical accumulation sites and fluorescence contrast levels. In closing, some comments are presented relating to technical design specifications future systems should have in order to allow them to successfully emerge as versatile whole-body fluorescence imaging tools. These final comments are divided into two categories, namely, specificity and sensitivity.

Specificity—A more universal imaging methodology will require the use of instrumentation (illumination and detection sub-assemblies) versatile enough to image at multiple wavelengths allowing the separation of different fluorophore species or removal of non-specific signals. In a very concrete example, spectral versatility allows the development of methods to isolate and remove the contribution of tissue autofluorecence. As discussed earlier, increasing the specificity of the technology can be achieved through multiplexing, but perhaps most effectively through the use of multi-spectral illumination and/or detection, as well as through the use of lifetime imaging based on time-domain detection.

Sensitivity—Another aspect than should be addressed in order to develop approaches that are as universal as possible consists in maximizing the sensitivity of the technology. High enough sensitivity would allow systems to acquire fluorescence signals transmitted through small animals with sufficient signal-to-noise. Contrary to reflection signals, trans-illumination signals depend only weakly on the location of the fluorescent molecules. This makes surface-weighted epi-illumination configurations less attractive than planar trans-illumination or tomography geometries when the objective is to reduce the imaging constraints relating to fluorophore location. As pointed out earlier, the development of such systems involves highly sensitive detection based, e.g., on PMT's or low temperature cooled CCD cameras. Such detection characteristics are also desirable in order to allow an instrument to image fluorescence contrast as low as possible. In fact, as mentioned earlier, optimizing system design to image low fluorescence contrast in trans-illumination can be achieved by selecting detection methods with low noise characteristics and large dynamical range.

Acknowledgments

This work was supported by the National Institutes of Health (NIH) through Award Number K25CA138578 and Grant Numbers RO1CA109558 and RO1CA120368 from the National Cancer Institute (NCI). The authors would like to extend their gratitude to the companies (ART Advanced Research Technologies, Berthold Technologies, Caliper Life Sciences, CRi, Carestream Health, LI-COR Biosciences, UVP and VisEn Medical) who provided the images shown in Figure 5, as well as most of the information compiled in Table 1. Finally, the authors would like to thank Venkat Krishnaswamy for useful discussions and comments.

7. REFERENCES

1. Jacques SL, Pogue BW. Tuturial on diffuse light transport. Journal of Biomedical Optics. 2008; 13(4):041302. [PubMed: 19021310]
2. Swartling J, et al. Fluorescence spectra provide information on the depth of fluorescent lesions in tissue. Applied Optics. 2005; 44(10):1934–1941. [PubMed: 15813529]
3. Davis SC, et al. Contrast-Detail Analysis Characterizes Diffuse Optical Fluorescence Tomography Image Reconstruction. Journal of Biomedical Optics. 2005; 10(5):050501-1–3. [PubMed: 16292936]
4. Billinton N, Knight AW. Seeing the Wood through the Trees: A Review of Techniques for Distinguishing Green Fluorescent Protein from Endogenous Autofluorescence. Analytical Biochemistry. 2001; 291:175–197. [PubMed: 11401292]
5. Wagnieres GA, Star WM, Wilson BC. In vivo fluorescence spectroscopy and imaging for oncological applications. Photochemistry & Photobiology. 1998; 68(5):603–32. [PubMed: 9825692]

6. Mansfield JR, et al. Autofluorescence removal, multiplexing, and automated analysis methods for in-vivo fluorescence imaging. Journal of Biomedical Optics. 2005; 10(4):041207 1–9.
7. Davis SC, et al. Image guided diffuse optical fluorescence tomography implemented with Laplacian-type regularization. Optics Express. 2007; 15(7):4066–4082. [PubMed: 19532650]
8. Hillman EMC, Moore A. All-optical anatomical co-registration for molecular imaging of small animals using dynamic contrast. Nature Photonics. 2007; 1:526–530. [PubMed: 18974848]
9. Richards-Kortum R, Sevick-Muraca E. Quantitative optical spectroscopy for tissue diagnosis. Annual Review of Physical Chemistry. 1996; 47:555–606.
10. Jacques SL, Pogue BW. Tutorial on Diffuse Light Transport. Journal of Biomedical Optics. 2008; 13(14):041302. [PubMed: 19021310]
11. Pogue BW, Gibbs SL, Chen B. Fluorescence Imaging In Vivo: Raster Scanned Point-Source Imaging Provides More Accurate Quantification than Broad Beam Geometries. Tech. Cancer Res. Treat. 2004; 3(1):15–21.
12. Pogue BW, Burke GC. Fiber optic bundle design for quantitative fluorescence measurement from tissue. Appl. Opt. 1998; 37(31):7429–36. [PubMed: 18301577]
13. Soubret A, Ripoll J, Ntziachristos V. Accuracy of fluorescent tomography in the presence of heterogeneities: Study of the normalized born ratio. Ieee Transactions on Medical Imaging. 2005; 24(10):1377–1386. [PubMed: 16229423]
14. Sinaasappel M, Sterenborg HJCM. Quantification of the hematoporphyrin derivative by fluorescence measurement using dual-wavelength excitation and dual-wavelength detection. Appl. Opt. 1993; 32(4):541–548. [PubMed: 20802722]
15. Hillman EM, Moore A. All-optical anatomical co-registration for molecular imaging of small animals using dynamic contrast. Nat Photonics. 2007; 1(9):526–530. [PubMed: 18974848]
16. Takeda M, Mutoh K. Fourier transform profilometry for the automatic measurement of 3-D object shapes. Applied Optics. 1983; 22(24):3977–3982. [PubMed: 18200299]
17. Ntziachristos V, et al. Fluorescence molecular tomography resolves protease activity in vivo. Nature Medicine. 2002; 8(7):757–60.
18. McCann CM, et al. Combined magnetic resonance and fluorescence imaging of the living mouse brain reveals glioma response to chemotherapy. Neuroimage. 2009; 45(2):360–9. [PubMed: 19154791]
19. Gibbs-Strauss SL, et al. Noninvasive measurement of aminolevulinic acid-induced protoporphyrin IX fluorescence allowing detection of murine glioma in vivo. Journal of Biomedical Optics. 2009; 14(1):014007–1. [PubMed: 19256695]
20. Veiseh M, et al. Tumor paint: a chlorotoxin:Cy5.5 bioconjugate for intraoperative visualization of cancer foci. Cancer Res. 2007; 67(14):6882–8. [PubMed: 17638899]
21. Hyde D, et al. Hybrid FMT-CT imaging of amyloid-beta plaques in a murine Alzheimer's disease model. Neuroimage. 2009; 44(4):1304–11. [PubMed: 19041402]
22. Hintersteiner M, et al. In vivo detection of amyloid-beta deposits by near-infrared imaging using an oxazine-derivative probe. Nat Biotechnol. 2005; 23(5):577–83. [PubMed: 15834405]
23. Wang Q, et al. Visualizing localized dynamic changes during epileptic seizure onset in vivo with diffuse optical tomography. Med Phys. 2008; 35(1):216–24. [PubMed: 18293577]
24. Klohs J, et al. Near-infrared fluorescence imaging with fluorescently labeled albumin: a novel method for non-invasive optical imaging of blood-brain barrier impairment after focal cerebral ischemia in mice. J Neurosci Methods. 2009; 180(1):126–32. [PubMed: 19427539]
25. Klohs J, et al. In vivo imaging of the inflammatory receptor CD40 after cerebral ischemia using a fluorescent antibody. Stroke. 2008; 39(10):2845–52. [PubMed: 18635859]
26. Klohs J, et al. In vivo near-infrared fluorescence imaging of matrix metalloproteinase activity after cerebral ischemia. J Cereb Blood Flow Metab. 2009
27. Johnson ND, Duysen EG, Lockridge O. Intrathecal delivery of fluorescent labeled butyrylcholinesterase to the brains of butyrylcholinesterase knock-out mice: visualization and quantification of enzyme distribution in the brain. Neurotoxicology. 2009; 30(3):386–92. [PubMed: 19442823]

28. Pham W, et al. Crossing the blood-brain barrier: a potential application of myristoylated polyarginine for in vivo neuroimaging. Neuroimage. 2005; 28(1):287–92. [PubMed: 16040255]
29. Deguchi JO, et al. Inflammation in atherosclerosis: visualizing matrix metalloproteinase action in macrophages in vivo. Circulation. 2006; 114(1):55–62. [PubMed: 16801460]
30. Chen J, et al. In vivo imaging of proteolytic activity in atherosclerosis. Circulation. 2002; 105(23): 2766–71. [PubMed: 12057992]
31. Nahrendorf M, et al. Nanoparticle PET-CT imaging of macrophages in inflammatory atherosclerosis. Circulation. 2008; 117(3):379–87. [PubMed: 18158358]
32. Sosnovik DE, et al. Fluorescence tomography and magnetic resonance imaging of myocardial macrophage infiltration in infarcted myocardium in vivo. Circulation. 2007; 115(11):1384–91. [PubMed: 17339546]
33. Shepherd J, et al. A fluorescent probe for the detection of myeloperoxidase activity in atherosclerosis-associated macrophages. Chem Biol. 2007; 14(11):1221–31. [PubMed: 18022561]
34. Sosnovik DE, et al. Fluorescence Tomography and Magnetic Resonance Imaging of Myocardial Macrophage Infiltration in Infarcted Myocardium In Vivo. Circulation. 2007; 115:1384–1391. [PubMed: 17339546]
35. Nahrendorf M, et al. Dual channel optical tomographic imaging of leukocyte recruitment and protease activity in the healing myocardial infarct. Circ Res. 2007; 100(8):1218–25. [PubMed: 17379832]
36. Urano Y, et al. Selective molecular imaging of viable cancer cells with pH-activatable fluorescence probes. Nat Med. 2009; 15(1):104–9. [PubMed: 19029979]
37. Haller J, et al. Visualization of pulmonary inflammation using noninvasive fluorescence molecular imaging. J Appl Physiol. 2008; 104:795–802. [PubMed: 18202169]
38. Grimm J, et al. Use of gene expression profiling to direct in vivo molecular imaging of lung cancer. Proc Natl Acad Sci U S A. 2005; 102(40):14404–9. [PubMed: 16183744]
39. Koenig A, et al. In vivo mice lung tumor follow-up with fluorescence diffuse optical tomography. Journal of Biomedical Optics. 2008; 13(1):011008 1–9. [PubMed: 18315357]
40. Grimm J, et al. Use of gene expression profiling to direct in vivo molecular imaging of lung cancer. PNAS. 2005; 102(40):14404–14409. [PubMed: 16183744]
41. Cortez-Retamozo V, et al. Real-time assessment of inflammation and treatment response in a mouse model of allergic airway inflammation. J Clin Invest. 2008; 118(12):4058–66. [PubMed: 19033674]
42. Montet X, et al. Tomographic fluorescence imaging of tumor vascular volume in mice. Radiology. 2007; 242(3):751–8. [PubMed: 17325064]
43. von Burstin J, et al. Highly sensitive detection of early-stage pancreatic cancer by multimodal near-infrared molecular imaging in living mice. Int J Cancer. 2008; 123(9):2138–47. [PubMed: 18709639]
44. Snyder CS, et al. Complementarity of ultrasound and fluorescence imaging in an orthotopic mouse model of pancreatic cancer. BMC Cancer. 2009; 9:106. [PubMed: 19351417]
45. Wack S, et al. Feasibility, sensitivity, and reliability of laser-induced fluorescence imaging of green fluorescent protein-expressing tumors in vivo. Mol Ther. 2003; 7(6):765–73. [PubMed: 12788650]
46. Samkoe, K., et al. Pancreas tumor response to verteporfin photodynamic therapy shows EGF activity change as well as tumor size reduction. 2009. (submitted, 2009)
47. Kobayashi H, et al. Multimodal nanoprobes for radionuclide and five-color near-infrared optical lymphatic imaging. ACS Nano. 2007; 1(4):258–64. [PubMed: 19079788]
48. Hama Y, et al. Two-color lymphatic mapping using Ig-conjugated near infrared optical probes. J Invest Dermatol. 2007; 127(10):2351–6. [PubMed: 17522707]
49. Hama Y, et al. Spectral near-infrared fluorescence imaging of curved surfaces using projection reconstruction algorithms. Contrast Media Mol Imaging. 2007; 2(2):82–7. [PubMed: 17451166]
50. Talanov VS, et al. Dendrimer-based nanoprobe for dual modality magnetic resonance and fluorescence imaging. Nano Lett. 2006; 6(7):1459–63. [PubMed: 16834429]

51. Garofalakis A, et al. Three-Dimensional In Vivo Imaging of Green Fluorescent Protein-Expressing T Cells in Mice with Noncontact Fluorescence Molecular Tomography. Molecular Imaging. 2007; 6(2):96–107. [PubMed: 17445504]
52. Martin A, et al. Imaging changes in lymphoid organs in vivo after brain ischemia with three-dimensional fluorescence molecular tomography in transgenic mice expressing green fluorescent protein in T lymphocytes. Mol Imaging. 2008; 7(4):157–67. [PubMed: 19123986]
53. Swirski FK, et al. A near-infrared cell tracker reagent for multiscopic in vivo imaging and quantification of leukocyte immune responses. PLoS ONE. 2007; 2(10):e1075. [PubMed: 17957257]
54. Christen T, et al. Molecular imaging of innate immune cell function in transplant rejection. Circulation. 2009; 119(14):1925–32. [PubMed: 19332470]
55. Kozloff KM, Weissleder R, Mahmood U. Noninvasive optical detection of bone mineral. J Bone Miner Res. 2007; 22(8):1208–16. [PubMed: 17488196]
56. Zaheer A, et al. In vivo near-infrared fluorescence imaging of osteoblastic activity. Nat Biotechnol. 2001; 19(12):1148–54. [PubMed: 11731784]
57. Aikawa E, et al. Osteogenesis associates with inflammation in early-stage atherosclerosis evaluated by molecular imaging in vivo. Circulation. 2007; 116(24):2841–50. [PubMed: 18040026]
58. Zilberman Y, et al. Fluorescence molecular tomography enables in vivo visualization and quantification of nonunion fracture repair induced by genetically engineered mesenchymal stem cells. J Orthop Res. 2008; 26(4):522–30. [PubMed: 17985393]
59. Kozloff KM, et al. Non-invasive optical detection of cathepsin K-mediated fluorescence reveals osteoclast activity in vitro and in vivo. Bone. 2009; 44(2):190–8. [PubMed: 19007918]
60. Mitsiades CS, et al. Fluorescence imaging of multiple myeloma cells in a clinically relevant SCID/NOD in vivo model: biologic and clinical implications. Cancer Res. 2003; 63(20):6689–96. [PubMed: 14583463]
61. Cross NA, et al. Imaging the effects of castration on bone turnover and hormone-independent prostate cancer colonization of bone. Prostate. 2008; 68(15):1707–14. [PubMed: 18726984]
62. Fournier PG, et al. Lowering bone mineral affinity of bisphosphonates as a therapeutic strategy to optimize skeletal tumor growth inhibition in vivo. Cancer Res. 2008; 68(21):8945–53. [PubMed: 18974139]
63. Wunder A, et al. In vivo imaging of protease activity in arthritis: a novel approach for monitoring treatment response. Arthritis & Rheumatism. 2004; 50(8):2459–65. [PubMed: 15334458]
64. Chen WT, et al. Arthritis imaging using a near-infrared fluorescence folate-targeted probe. Arthritis Res Ther. 2005; 7(2):R310–7. [PubMed: 15743478]
65. Izmailova ES, et al. Use of molecular imaging to quantify response to IKK-2 inhibitor treatment in murine arthritis. Arthritis Rheum. 2007; 56(1):117–28. [PubMed: 17195214]
66. Hama Y, et al. A self-quenched galactosamine-serum albumin-rhodamineX conjugate: a “smart” fluorescent molecular imaging probe synthesized with clinically applicable material for detecting peritoneal ovarian cancer metastases. Clin Cancer Res. 2007; 13(21):6335–43. [PubMed: 17975145]
67. Hama Y, et al. Targeted optical imaging of cancer cells using lectin-binding BODIPY conjugated avidin. Biochem Biophys Res Commun. 2006; 348(3):807–13. [PubMed: 16904640]
68. Xu H, et al. Preparation and preliminary evaluation of a biotin-targeted, lectin-targeted dendrimer-based probe for dual-modality magnetic resonance and fluorescence imaging. Bioconjug Chem. 2007; 18(5):1474–82. [PubMed: 17711320]
69. Gunn AJ, et al. Targeted optical fluorescence imaging of human ovarian adenocarcinoma using a galactosyl serum albumin-conjugated fluorophore. Cancer Sci. 2007; 98(11):1727–33. [PubMed: 17784874]
70. Hama Y, et al. A target cell-specific activatable fluorescence probe for in vivo molecular imaging of cancer based on a self-quenched avidin-rhodamine conjugate. Cancer Res. 2007; 67(6):2791–9. [PubMed: 17363601]
71. Kamiya M, et al. An enzymatically activated fluorescence probe for targeted tumor imaging. J Am Chem Soc. 2007; 129(13):3918–29. [PubMed: 17352471]

72. Hama Y, et al. D-galactose receptor-targeted in vivo spectral fluorescence imaging of peritoneal metastasis using galactosamin-conjugated serum albumin-rhodamine green. J Biomed Opt. 2007; 12(5):051501. [PubMed: 17994865]
73. Chang SK, et al. In vivo optical molecular imaging of vascular endothelial growth factor for monitoring cancer treatment. Clin Cancer Res. 2008; 14(13):4146–53. [PubMed: 18593993]
74. Bogdanov AA Jr. Lin CP, Kang HW. Optical imaging of the adoptive transfer of human endothelial cells in mice using anti-human CD31 monoclonal antibody. Pharm Res. 2007; 24(6): 1186–92. [PubMed: 17373582]
75. Cai W, et al. Peptide-labeled near-infrared quantum dots for imaging tumor vasculature in living subjects. Nano Lett. 2006; 6(4):669–76. [PubMed: 16608262]
76. Mayes P, et al. Noninvasive vascular imaging in fluorescent tumors using multispectral unmixing. Biotechniques. 2008; 45(4):459–60. 461–4. [PubMed: 18855773]
77. Hama Y, et al. Two-color in vivo dynamic contrast-enhanced pharmacokinetic imaging. J Biomed Opt. 2007; 12(3):034016. [PubMed: 17614724]
78. Caceres G, et al. Imaging of luciferase and GFP-transfected human tumours in nude mice. Luminescence. 2003; 18(4):218–23. [PubMed: 12950058]
79. Diehn FE, et al. Noninvasive fluorescent imaging reliably estimates biomass in vivo. Biotechniques. 2002; 33(6):1250–2. 1254–5. [PubMed: 12503309]
80. Choy G, et al. Comparison of noninvasive fluorescent and bioluminescent small animal optical imaging. Biotechniques. 2003; 35(5):1022–6. 1028–30. [PubMed: 14628676]
81. Yang M, et al. Visualizing gene expression by whole-body fluorescence imaging. Proc Natl Acad Sci U S A. 2000; 97(22):12278–82. [PubMed: 11050247]
82. Vera DR, et al. Cy5.5-DTPA-galactosyl-dextran: a fluorescent probe for in vivo measurement of receptor biochemistry. Nucl Med Biol. 2005; 32(7):687–93. [PubMed: 16243643]
83. Su J, et al. Exploring feasibility of multicolored CdTe quantum dots for in vitro and in vivo fluorescent imaging. J Nanosci Nanotechnol. 2008; 8(3):1174–7. [PubMed: 18468119]
84. Zhang J, et al. Evaluation of red CdTe and near infrared CdHgTe quantum dots by fluorescent imaging. J Nanosci Nanotechnol. 2008; 8(3):1155–9. [PubMed: 18468115]
85. Gao X, et al. In vivo cancer targeting and imaging with semiconductor quantum dots. Nat Biotechnol. 2004; 22(8):969–76. [PubMed: 15258594]
86. Bullok KE, et al. Biochemical and in vivo characterization of a small, membrane-permeant, caspase-activatable far-red fluorescent peptide for imaging apoptosis. Biochemistry. 2007; 46(13): 4055–65. [PubMed: 17348687]
87. von Wallbrunn A, et al. In vivo optical imaging of CD13/APN-expression in tumor xenografts. Journal of Biomedical Optics. 2008; 13(1):011077 1–9.
88. Koyama Y, et al. In vivo molecular imaging to diagnose and subtype tumors through receptor-targeted optically labeled monoclonal antibodies. Neoplasia. 2007; 9(12):1021–9. [PubMed: 18084609]
89. Barrett T, et al. In vivo diagnosis of epidermal growth factor receptor expression using molecular imaging with a cocktail of optically labeled monoclonal antibodies. Clin Cancer Res. 2007; 13(22 Pt 1):6639–48. [PubMed: 17982120]
90. Gee MS, et al. Human breast cancer tumor models: molecular imaging of drug susceptibility and dosing during HER2/neu-targeted therapy. Radiology. 2008; 248(3):925–35. [PubMed: 18647846]
91. Bremer C, et al. Optical imaging of matrix metalloproteinase-2 activity in tumors: feasibility study in a mouse model. Radiology. 2001; 221(2):523–9. [PubMed: 11687699]
92. Daldrup-Link HE, et al. Cell tracking with gadophrin-2: a bifunctional contrast agent for MR imaging, optical imaging, and fluorescence microscopy. Eur J Nucl Med Mol Imaging. 2004; 31(9):1312–21. [PubMed: 15138719]
93. Lisy MR, et al. In vivo near-infrared fluorescence imaging of carcinoembryonic antigen-expressing tumor cells in mice. Radiology. 2008; 247(3):779–87. [PubMed: 18413884]
94. Duysen EG, Lockridge O. Whole body and tissue imaging of the butyrylcholinesterase knockout mouse injected with near infrared dye labeled butyrylcholinesterase. Chem Biol Interact. 2008; 175(1-3):119–24. [PubMed: 18486120]

95. Zacharakis G, et al. Normalized Transillumination of Fluorescent Proteins in Small Animals. Molecular Imaging. 2006; 5(3):153–159. [PubMed: 16954030]
96. Wall A, et al. Differentiation of angiogenic burden in human cancer xenografts using a perfusion-type optical contrast agent (SIDAG). Breast Cancer Res. 2008; 10(2):R23. [PubMed: 18331624]
97. Montet X, et al. Tomographic fluorescence mapping of tumor targets. Cancer Res. 2005; 65(14): 6330–6. [PubMed: 16024635]
98. von Wallbrunn A, et al. In vivo imaging of integrin alphav-beta3 expression using fluorescence-mediated tomography. Eur. J. Nucl. Med. Mol. Imaging. 2007; 34:745–754. [PubMed: 17131149]
99. Bremer C, Ntziachristos V, Weissleder R. Optical-based molecular imaging: contrast agents and potential medical applications. European Radiology. 2003; 13(2):231–43. [PubMed: 12598985]
100. Weissleder R, Mahmood U. Molecular imaging. Radiology. 2001; 219(2):316–33. [PubMed: 11323453]
101. Weissleder R. Molecular imaging: exploring the next frontier. Radiology. 1999; 212(3):609–14. [PubMed: 10478223]
102. Hoffman RM. A better fluorescent protein for whole-body imaging. Trends in Biotechnology. 2008; 26(1):1–4. [PubMed: 18037177]
103. Schcherbo D, et al. Bright fard-red fluorescent protein for whole-body imaging. Nature Methods. 2007; 4(9):741–746. [PubMed: 17721542]
104. Shkrob MA, et al. Far-red flurorescent proteins evolved from a blue chromoprotein from Actinia equina. Biochem. J. 2005; 392:649–654. [PubMed: 16164420]
105. Shu X, et al. Mammalian Expression of Infrared Fluorescent Proteins Engineered from a Bacterial Phytochrome. Science. 2009; 324(804-807)
106. Hassan M, et al. Fluorescence lifetime imaging system for in vivo studies. Mol. Imaging. 2007; 6(4):229–236. [PubMed: 17711778]
107. Bloch S, et al. Whole-body fluorescence lifetime imaging of a tumor-targeted near-infrared molecular probe in mice. Journal of Biomedical Optics. 2005; 10(5):054003. [PubMed: 16292963]
108. Hutchinson CL, Lakowicz JR, Sevick-Muraca EM. Fluorescence lifetime-based sensing in tissues: a computational study. Biophys. J. 1995; 68(4):1574–1582. [PubMed: 7787043]
109. Kuwana E, Sevick-Muraca EM. Fluorescence lifetime spectroscopy in multiply scattering media with dyes exhibiting multiexponential decay kinetics. Biophysical Journal. 2002; 83(2):1165–76. [PubMed: 12124296]
110. Hattery D, et al. Analytical solutions for time-resolved fluorescence lifetime imaging in a turbid medium such as tissue. J. Opt. Soc. Am. A. 2001; 18(7):15231530.
111. Gruber, J., et al. System for Fluorescence Quantification of Thin Tissue Layers Guided by High Frequency Ultrasound. in SPIE BiOS: Optical Methods for Tumor Treatment and Detection: Mechanisms and Techniques in Photodynamic Therapy XVIII. SPIE Press; San Jose: 2009.
112. Zacharakis G, et al. Fluorescent protein tomography scanner for small animal imaging. Ieee Transactions on Medical Imaging. 2005; 24(7):878–885. [PubMed: 16011317]
113. Deliolanis N, et al. Free-space fluorescence molecular tomography utilizing 360 degrees geometry projections. Optics Letters. 2007; 32(4):382–384. [PubMed: 17356660]
114. Ntziachristos V, Weissleder R. Charge-coupled-device based scanner for tomography of fluorescent near-infrared probes in turbid media. Medical Physics. 2002; 29(5):803–9. [PubMed: 12033576]
115. Patwardhan SV, et al. Time-dependent whole-body fluorescence tomography of probe bio-distribution in mice. Optics Express. 2005; 13(7):2564–2577. [PubMed: 19495147]
116. Graves EE, et al. A submillimeter resolution fluorescence molecular imaging system for small animal imaging. Med. Phys. 2003; 30(5):901–911. [PubMed: 12772999]
117. Davis SC, et al. Magnetic resonance-coupled fluorescence tomography scanner for molecular imaging of small animals and human breasts. Rev. Sci. Instr. 2008 (in press).
118. Zavattini G, et al. A hyperspectral fluorescence system for 3D in vivo optical imaging. Phys. Med. Biol. 2006; 51:2029–2043. [PubMed: 16585843]

119. Leavesley S, et al. An excitation wavelength-scanning spectral imaging system for preclinical imaging. Review of Scientific Instruments. 2008; 79:023707–1. 023707–10. [PubMed: 18315305]
120. Li C, et al. A three-dimensional multispectral fluorescence optical tomography imaging system for small animals based on a conical mirror design. Optics Express. 2009; 17(9):7571–7585. [PubMed: 19399136]
121. Kepshire DS, et al. A microcomputed tomography guided fluorescence tomography system for small animal molecular imaging. Review of Scientific Instruments. 2009; 80:043701. [PubMed: 19405660]
122. Brambilla M, et al. Time-resolved scanning system for double reflectance and transmittance fluorescence imaging of diffusive media. Review of Scientific Instruments. 2008; 79:013103 1–9. [PubMed: 18248018]
123. Kumar ATN, et al. A Time Domain Fluorescence Tomography System for Small Animal Imaging. IEEE Transactions on Medical Imaging. 2008; 27(8):1152–1163. [PubMed: 18672432]
124. Niedre MJ, et al. Early photon tomography allows fluorescence detection of lung carcinomas and disease progression in mice in vivo. PNAS. 2008; 105(49):19126–19131. [PubMed: 19015534]
125. Lam S, Lesage F, Intes X. Time Domain Fluorescent Diffuse Optical Tomography: analytical expressions. Optics Express. 2005; 13:2263–2275. [PubMed: 19495115]
126. Riley J, et al. Choice of data types in time resolved fluorescence enhanced diffuse optical tomography. Med. Phys. 2007; 34(12):4890–4900. [PubMed: 18196814]
127. Leblond F, et al. Early photons fluorescence tomography: spatial resolution improvements and noise stability considerations. J. Opt. Soc. Am. A. 2009 doc. ID 108321 (in press).
128. Kepshire D, et al. Fluorescence tomography characterization for sub-surface imaging with protoporphyrin IX. Optics Express. 2008; 16(12):8581–8593. [PubMed: 18545571]
129. Chang JH, Graber HL, Barbour RL. Imaging of fluorescence in highly scattering media. IEEE Trans. Biomed. Eng. 1997; 44(9):810–822. [PubMed: 9282473]
130. Chang J, Graber HL, Barbour RL. Luminescence optical tomography of dense scattering media. J. Opt. Soc. Am. A. 1997; 14(1):288–99.
131. Herve L, et al. Noncontact fluorescence diffuse optical tomography of heterogeneous media. Applied Optics. 2007; 46(22):4896–4906. [PubMed: 17676093]
132. Hyde D, et al. A Statistical Approach to Inverting the Born Ratio. IEEE Transactions on Medical Imaging. 2007; 26(7):893–905. [PubMed: 17649903]
133. Joshi A, Bangerth W, Sevick-Muraca EM. Adaptative finite element based tomography for fluorescence optical imaging in tissue. Optics Express. 2004; 12(22):5402–5417. [PubMed: 19484100]
134. Joshi A, Bangerth W, Sevick-Muraca EM. Non-contact fluorescence optical tomography with scanning patterned illumination. Optics Express. 2006; 14(14):6516–6534. [PubMed: 19516829]
135. Joshi A, et al. Plane-wave fluorescence tomography with adaptative finute elements. Optics Letters. 2006; 31(2):193–195. [PubMed: 16441027]
136. Lasser T, Ntziachristos V. Optimization of 360 degrees projection fluorescence molecular tomography. Medical Image Analysis. 2007; 11:389–399. [PubMed: 17524701]
137. Lee J, Sevick-Muraca EM. Three-dimensional fluorescence enhanced optical tomography using referenced frequency-domain photon migration measurements at emission and excitation wavelengths. Journal of the Optical Society of America, A, Optics, Image Science, & Vision. 2002; 19(4):759–71.
138. L'Huillier J-P, Vaudelle F. Improved localization of hidden fluorescent objects in highly scattering slab media based on a two-way transmittance determination. Optics Express. 2006; 14(26):12915–12929. [PubMed: 19532185]
139. Mohajerani P, et al. Optimal sparse solution for fluorescent diffuse optical tomography: theory and phantom experimental results. Applied Optics. 2007; 46(10):1679–85. [PubMed: 17356610]
140. Mohajerani P, Eftekhar AA, Adibi A. Object localization in the presence of a strong heterogenous background in fluorescent tomography. J. Opt. Soc. Am. A. 2008; 25(6):1467–1479.

141. Schulz RB, et al. Comparison of noncontact and fiber-based fluorescence-mediated tomography. Optics Letters. 2006; 31(6):769–771. [PubMed: 16544618]
142. Schulz RB, Ripoll J, Ntziachristos V. Experimental fluorescence tomography of tissues with noncontact measurements. IEEE Transactions on Medical Imaging. 2004; 23(4):492–500. [PubMed: 15084074]
143. Cong AX, Wang G. A finite-element-based reconstruction method for 3D fluorescence tomography. Optics Express. 2005; 13(24):9847–9857. [PubMed: 19503194]
144. Song X, et al. Reconstruction for free-space fluorescence tomography using a novel hybrid adaptive finite element algorithm. Optics Express. 2007; 15(26):18300–18317. [PubMed: 19551128]
145. Soubret A, Ntziachristos V. Fluorescence molecular tomography in the presence of background fluorescence. Phys. Med. Biol. 2006; 51:3983–4001. [PubMed: 16885619]
146. Wang D, Song X, Bai J. Adaptative-mesh-based algorithm for fluorescence molecular tomography using an analytical solution. Optics Express. 2007; 15(15):9722–9730. [PubMed: 19547322]
147. Wang D, Song X, Bai J. Adaptative-mesh-based algorithm for fluorescence molecular tomography using an analytical solution: erratum. Optics Express. 2007; 15(17):10789. [PubMed: 19547435]
148. Zou W, Wang J, Feng DD. Fluorescent molecular tomographic image reconstruction based on the Green's function. J. Opt. Soc. Am. A. 2007; 24(7):2014–2022.
149. Graves EE, et al. Singular-value analysis and optimization of experimental parameters in fluorescence molecular tomography. Journal of the Optical Society of America, A, Optics, Image Science, & Vision. 2004; 21(2):231–41.
150. Graves EE, et al. Validation of in vivo fluorochrome concentrations measured using fluorescence molecular tomography. Journal of Biomedical Optics. 2005; 10(4):044019 1–10.
151. Eppstein MJ, et al. A comparison of exact and approximate adjoint sensitivities in fluorescence tomography. IEEE Transactions on Medical Imaging. 2003; 22(10):1215–23. [PubMed: 14552576]
152. Fedele F, Laible JP, Eppstein MJ. Coupled complex adjoint sensitivities for frequency-domain fluorescence tomography: theory and vectorized implementation. Journal of Computational Physics. 2003; 187:597–619.
153. Klose AD, Hielscher AH. Fluorescence tomography with simulated data based on the equation of radiative transfer. Optics Letters. 2003; 28(12):1019–1021. [PubMed: 12836765]
154. Schulz RB, Ripoll J, Ntziachristos V. Noncontact optical tomography of turbid media. Optics Letters. 2003; 28(18):1701–3. [PubMed: 13677542]
155. Ntziachristos V, Weissleder R. Experimental three-dimensional fluorescence reconstruction of diffuse media by use of a normalized Born approximation. Optics Letters. 2001; 26(12):893–895. [PubMed: 18040483]
156. Chang J, Graber HL, Barbour RL. Improved reconstruction algorithm for luminescence optical tomography when background lumiphore is present. Applied Optics. 1998; 37(16):3547–3552. [PubMed: 18273322]
157. Gao M, et al. Effects of background fluorescence in fluorescence molecular tomography. Applied Optics. 2005; 44(26):5468–5474. [PubMed: 16161661]
158. Chaudhari AJ, et al. Hyperspectral and multispectral bioluminescence optical tomography for small animal imaging. Phys. Med. Biol. 2005; 50:5421–5441. [PubMed: 16306643]
159. Zacharopoulos A, et al. A matrix-free algorithm for multiple wavelength fluorescence tomography. Optics Express. 2009; 17(5):3025–3035. [PubMed: 19259141]
160. Axelsson J, Svensson J, Andersson-Engels S. Spatially varying regularization based on spectrally resolved fluorescence molecular tomography. Optics Express. 2007; 15(21):13574–13584. [PubMed: 19550625]
161. Quan H, Guo Z. Fast 3-D optical imaging with transient fluorescence signals. Optics Express. 2004; 12(3):449–457. [PubMed: 19474844]
162. Gao F, et al. A linear, featured-data scheme for image reconstruction in time-domain fluorescence molecular tomography. Optics Express. 2006; 14(16):7109–7124. [PubMed: 19529082]

163. Gao F, et al. A self-normalized, full time-resolved method for fluorescence diffuse optical tomography. Optics Express. 2008; 16(17):13104–13121. [PubMed: 18711549]
164. O'Leary MA, et al. Fluorescence lifetime imaging in turbid media. Opt. Lett. 1996; 21(2):158–160. [PubMed: 19865337]
165. Paithankar DY, et al. Imaging of fluorescent yield and lifetime from multiply scattered light reemitted from random media. Applied Optics. 1997; 36(10):2260–2272. [PubMed: 18253202]
166. Shives E, Xu Y, Jiang H. Fluorescence lifetime tomography of turbid media based on an oxygen-sensitive dye. Optics Express. 2002; 10(26):1557–1562. [PubMed: 19461692]
167. Chang JW, Graber HL, Barbour RL. Luminescence optical tomography of dense scattering media. Journal of the Optical Society of America a-Optics Image Science and Vision. 1997; 14(1):288–299.
168. Milstein AB, et al. Fluorescence optical diffusion tomography using multiple-frequency data. Journal of the Optical Society of America, A, Optics, Image Science, & Vision. 2004; 21(6): 1035–49.
169. Roy R, Sevick-Muraca EM. Truncated Newton's optimization scheme for absorption and fluorescence optical tomography: Part II reconstruction from synthetic measurements. Optics Express. 1999; 4(10):372–382. [PubMed: 19396293]
170. Soloviev VY. Mesh adaptation technique for Fourier-domain fluorescence lifetime imaging. Med. Phys. 2006; 33(11):4176–4183. [PubMed: 17153396]
171. Soloviev VY, et al. Fluorescence lifetime imaging by using time-gated data acquisition. Applied Optics. 2007; 46(30):7384–7391. [PubMed: 17952172]
172. Godavarty A, Sevick-Muraca EM, Eppstein MJ. Three-dimensional fluorescence lifetime tomography. Medical Physics. 2005; 32(4):992–1000. [PubMed: 15895582]
173. Lin Y, Gao H, Gulsen G. Fluorescence diffuse optical tomography with functional and anatomical a priori information: feasibility study. Phys. Med. Biol. 2007; 52:5569–5585. [PubMed: 17804882]
174. Lin Y, et al. Wuantitative fluorescence tomography with functional and structural a priori information. Applied Optics. 2009; 48(7):1328–1336. [PubMed: 19252634]
175. Tan Y, Jiang H. DOT guided fluorescence molecular tomography or arbitrarily shaped objects. Med. Phys. 2008; 35(12):5703–5707. [PubMed: 19175127]
176. Tan Y, Jiang H. Diffuse optical tomography guided quantitative fluorescence molecular tomography. Applied Optics. 2008; 47(12):2011–2016. [PubMed: 18425173]
177. Niedre M, Ntziachristos V. Elucidating Structure and Function In Vivo With Hybrid Fluorescence and Magnetic Resonance Imaging. Proceedings of the IEEE. 2008; 96(3):382–387.
178. Tran Cao HS, et al. Development of the Transgenic Cyan Fluorescent Protein (CFP)-Expressing Nude Mouse for "Technicolor" Cancer Imaging. Journal of Cellular Biochemistry. 2009; 107:328–334. [PubMed: 19306297]

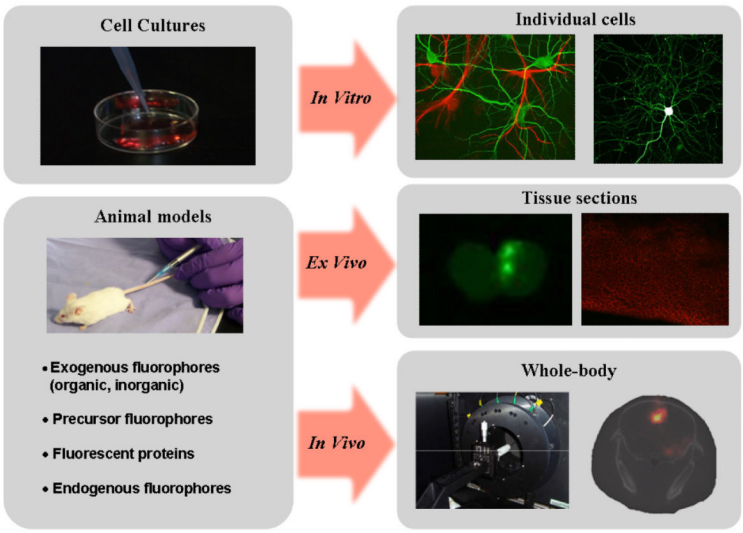

Figure 1.

Illustration showing different fluorescence imaging paths used in the scope of preclinical studies. High resolution, high sensitivity and high specificity images can be rendered down to sub-micron resolution in vitro to study cellular and sub-cellular molecular processes. The top-right part of the figure shows two-photon microscopy images of mouse hippocampal neuron and glial cells transfected with GFP and RFP, respectively (*courtesy of Dr Paul De Koninck, www.greenspine.ca*). Animal models can be used for ex vivo studies of tissue slices as well as for whole-body in vivo studies. Ex vivo slices shown (middle-right images) correspond to brain tissue with glioma cells highlighted with fluorescence from GFP and the endogenous molecule Protoporphyrin IX. The in vivo whole-body image (lower-right in the figure) corresponds to a fluorescence tomography image associated with PpIX contrast from a brain tumor model.

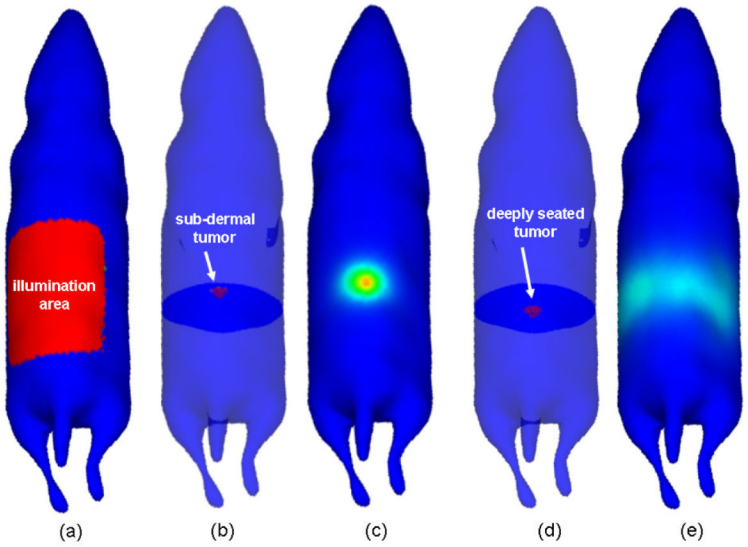

Figure 2.

Images showing the impact photon scattering can have on fluorescence imaging in living tissue. Two numerically simulated mouse models were used. An 8 mm diameter spherical tumor was located in the abdomen in each simulated mouse: (b) near the surface, (d) close to the axial center of the animal. Simulation results are shown for broad beam epi-illumination imaging: (a) shows the illuminated area on the surface of the animal while (c) and (e) show the outgoing light at the surface for the tumors shown in (b) and (d), respectively. In both cases, no background fluorescence was assumed. The intensity of the outgoing light in (e) is approximately one-thousandth of that shown in (c).

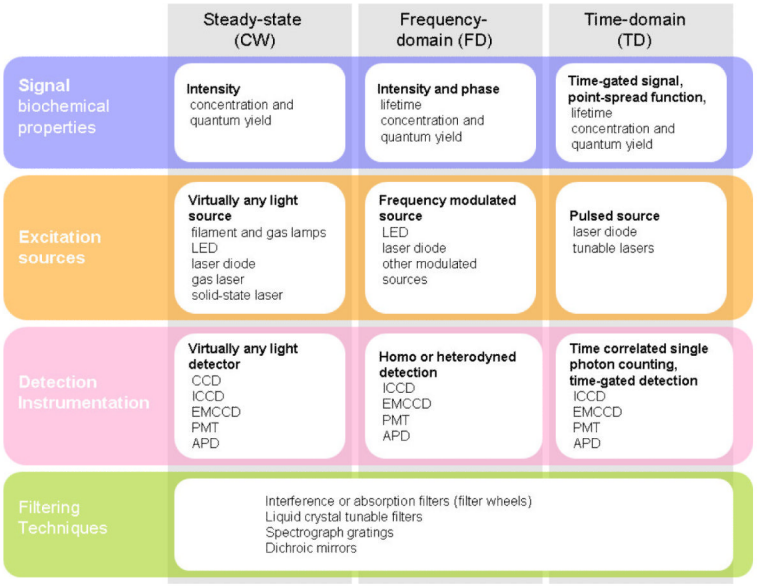

Figure 3.

Three major hardware design strategies for in vivo fluorescence imaging are shown in the columns of the table. Comparison of the imaging approaches is provided in terms of the main four components needed for each. They are listed in the rows where the intersection boxes detail the relevant data or components.

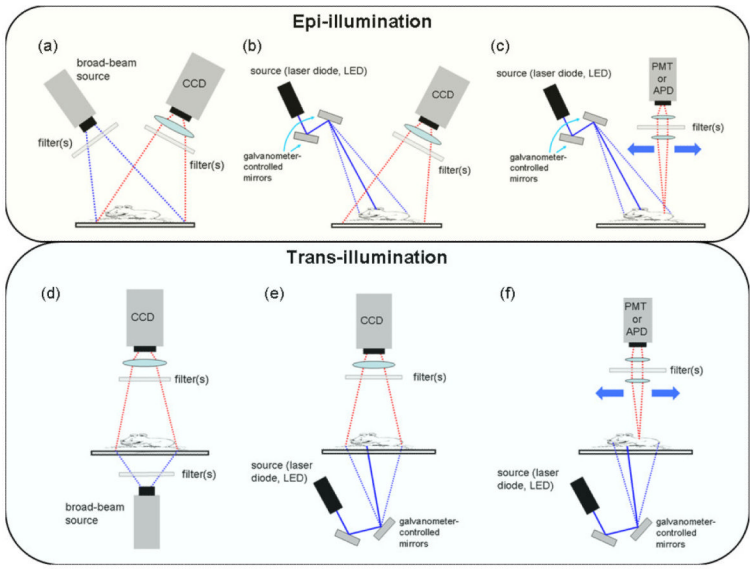

Figure 4.

Schematic rendering of different methods that can be used for whole-body fluorescence imaging. The first row shows epi-illumination geometries: (a) broad beam illumination with wide-field camera detection; (b) raster-scan illumination with wide-field camera detection, (c) raster-scan illumination and detection. The lower row of images shows the corresponding trans-illumination configurations. Not shown in the figure are configurations optimized for tomography imaging and fiber-based planar configurations.

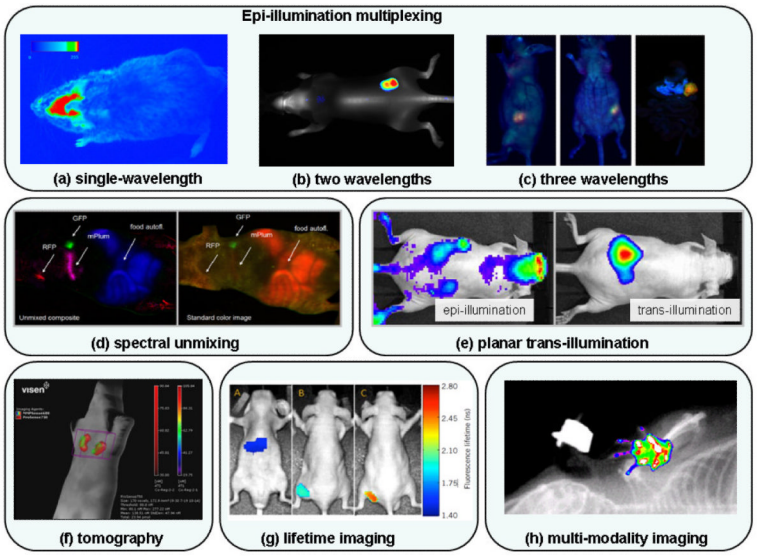

Figure 5.

Whole-body fluorescence images acquired in vivo with existing commercial systems: (a) Single-wavelength image (excitation: ~680 nm, emission: ~720 nm) of an oxazine-derivate dye binding to beta-amyloid deposits present in Alzheimer's disease (NightOWL-LB 983, courtesy of Berthold Technologies). (b) Tumor grown sub-cutaneously on right hip from A431 tumor cells. Image shows contrast associated with IRDye680 BoneTag (grayscale, excitation: 680 nm, emission: ~700 nm) and IRDye800CW EGF (pseudo-color, excitation: 780 nm, emission: ~800 nm) (Pearl Imager, courtesy of LI-COR Biosciences). (c) Imaging of XPA-1 tumors grown orthotopically in transgenic CFP nude mice from pancreatic cancer cells transfected with two fluorescent proteins to express GFP in the nucleus and RFP in the cytoplasm. Images show the dual-colored tumor in red (RFP) and green (GFP) color scales, while the pancreas and rest of the mouse appear in blue from the CFP [178] (iBox). (d) Images from a nude mouse with three sub-dermal tumors labeled with fluorescent proteins. The left-most image shows a representation of the fluorescence emanating from the animal (no spectral decomposition) while the other image is a composite combining the spectrally unmixed GFP, RFP and mPlum-FP images (green, red and magenta color scales, respectively) and the food autofluorescence (in blue) [6] (Maestro). (e) Images of approximately 1×10^{13} quantum dots (excitation: ~800 nm) implanted medial to the left kidney. The deeply-seated distribution of fluorescent molecules cannot be distinguished from autofluorescence sources in the epi-illumination image (left) but is clearly visible on the trans-illumination image (right) (IVIS Spectrum, courtesy of Caliper Life Sciences). (f) Multiplexed quantification of metalloproteinase and cathepsin activity in 4T1 mammary fat pas tumors. Fluorescence tomography image shows contrast from agents ProSense 750 (distributed throughout the tumor – red color scale) and MMPSense 680 (distributed on the surface of the tumor - in green) (FT 2500, courtesy of VisEn Medical). (g) Simultaneous lifetime imaging of two molecular biomarkers binding to cancer in xenograft mouse model (U-87MG glioblastoma cell line with mutation in EGF receptor) injected in flank of a nude mouse: lifetime of C225-Cy5.5 (C225 antibody-Cetuximab, an EGFR targeting antibody) in liver (image A), in the tumor (image B) and of Tf-DY682 (transferrin protein binding to transferrin receptors) in the tumor (image C) (Optix MX2, courtesy of ART Advanced Research and Technologies). (h) Combined digital X-ray image fluorescence image (excitation: ~720nm, emission: ~790nm) (KODAK In Vivo Imaging System, courtesy of Carestream Health).

Table 1

Summary of the main technical features associated with high-end commercially available in vivo whole-body fluorescence imaging systems. Most companies offer less expensive versions of these instruments which do not include all of the features presented in the table. Not included in the table is the Photon Imager system from Biospace Lab. The main distinguishing feature of this instrument is that fluorescence is detected with an ICCD camera potentially providing increased sensitivity compared to conventional cooled CCD cameras. Also, Caliper Life Sciences offers an epi-illumination fluorescence system integrating planar X-ray imaging for structural co-registration.

Instrument (Company)		**Optix MX3 (ART)**	**NightOWL II - LB 983 NC 100 (Berthold Tech.)**	**IVIS Spectrum (Caliper Life Sciences)**	**Maestro (CRi)**	**KODAK In-Vivo Imaging System (Carestream Health)**	**Pearl Imager (LI-COR Biosciences)**	**iBox (UVP)**	**FMT 2500LX (VisEn Medical)**
Applications	**Planar Mode**	epi-illumination	epi-illumination	epi-illumination & trans-illumination	epi-illumination	epi-illumination	epi-illumination	epi-illumination	epi-illumination
	Multiplexing	yes (limited by scan time)	yes (>2 wavelengths)	yes (>2 wavelengths)	yes (>2 wavelengths)	yes (>2 wavelengths)	yes (2 wavelengths)	yes (>2 wavelengths)	yes (4 wavelengths)
	Multi-fluorophore separation	lifetime imaging	---	spectral unmixing	spectral unmixing	spectral unmixing	---	spectral unmixing	---
	3D	topography (depth calculation)	---	tomography	---	---	---	---	tomography
	Surface Rendering	yes	no	yes	no	no	no	no	yes
Illumination	**light source**	pulsed laser diodes (300-800 μW) external CW tunable laser	tungsten lamp (75 W)	tungsten lamp (150 W)	xenon-halogen lamp (300 W)	halogen (150 W) or xenon lamp (175 W)	laser diodes	halogen lamp (150 W)	laser diodes LEDs
	wavelengths	470, 532, 635, 670, 735, 785 nm (up to 4 internal lasers)	340-1100 nm (selectable, 4 filter positions)	430-840 nm (selectable, 28 filter positions)	455-780 nm (selectable, 9 filter positions)	385-770 nm (selectable, 29 filter positions)	680, 780 nm	365-750 nm (selectable, 8 filter positions)	635, 670,745,785 nm
	method	epi-illumination (raster-scanning)	epi-illumination (broad beam)	epi-illumination (broad beam) transillumination (raster-scanning)	epi-illumination (broad beam)	epi-illumination (broad beam)	epi-illumination (NA)	epi-illumination (broad beam)	epi-illumination (broad beam, LEDs) trans-illumination (laser scanning)
Detection	**technology**	PMT TCSPC	CCD cooled −80 to −90°C 1.0 MP (13μm) 16-bit digitizer	CCD cooled −90°C 4.2MP (13.5μm) 16-bit digitizer	CCD cooled 0°C or +8°C 1.4 MP (6.5μm) 12-bit digitizer	CCD cooled −29°C 4.2 MP (10μm) 16-bit digitizer	CCD (details NA)	CCD cooled −28°C 4.2 MP (7.4μm) 16-bit digitizer	CCD cooled 16-bit digitizer
	wavelengths (filtering)	450-900 nm (selectable, 24 filter positions)	300-1050 nm (selectable, 4 filter positions)	300-1100 nm (selectable, 28 filter positions)	500-950 nm (continuous, liquid crystal tunable filters, 20 or 40 nm resolution, 1nm steps)	440-830 nm (selectable, 4 filter positions)	700, 800 nm (selectable, 2 filter positions)	450-850 nm (5 filter positions)	700, 800 nm (selectable, 8 filter positions)
	FOV (optics)	20×8.4 cm^2 (raster-scan detection - 0.5–3 mm resolution)	1×1 to 25×25 cm^2 (motorized camera, lens setting for magnification, focus	4×4 to 25×25 cm^2 (lens settings for magnification, focus adjustment)	11.2×8.4 cm^2 (max.) (lens settings for magnification, focus adjustment)	2×2 to 20×20 cm^2 (lens settings for magnification, focus adjustment)	12×9 cm^2 (NA)	8×8 - 16×16 cm^2 or 14×14 - 30×30 cm^2 (lens settings for magnification, focus	8×8 cm^2 (epi-illumination) 5×5 cm^2 (trans-illumination)

Instrument (Company)		Optix MX3 (ART)	NightOWL II - LB 983 NC 100 (Berthold Tech.)	IVIS Spectrum (Caliper Life Sciences)	Maestro (CRi)	KODAK In-Vivo Imaging System (Carestream Health)	Pearl Imager (LI-COR Biosciences)	iBox (UVP)	FMT 2500LX (VisEn Medical)
			adjustment)					adjustment)	
Multi-modal imaging	**While light image**	Yes	Yes	Yes	Yes	---	Yes	Yes	Yes
	Bioluminescence	Yes	Yes	Yes	---	---	---	---	---
	Multimodal	CT-coupling stage	CT, MRI, PET/SPECT, US	CT, MRI, digital mouse atlas	---	X-ray, radioisotopic detection (planar)	---	---	adapters for CT, MRI, PET/SPECT
	Co-registration software	Yes (to CT imaging)	Yes	Yes	---	Yes (automated to planar X-ray images)	---	---	Yes
Animal Handling	**Anesthesia hook-up**	Yes	Yes	Yes	Yes	Yes	Yes	Yes	Yes
	Temperature control	Yes (heated stage)	Yes (heated stage)	Yes (heated stage)	Yes (heated stage)	Yes (heated chamber)	Yes (heated stage)	Yes (heated stage)	Yes (heated chamber)
	Number per image	up to 5	up to 2	up to 5	up to 3	NA	1	up to 3	1